Chemosphere 366 (2024) 143465

Contents lists available at ScienceDirect

Chemosphere

journal homepage: www.elsevier.com/locate/chemosphere

The recent development of innovative photoelectro-Fenton processes for the effective and cost-effective remediation of organic pollutants in waters

Enric Brillas [a,*], Juan M. Peralta-Hernandez [b,**]

[a] Departament de Ciència de Materials i Química Física, Facultat de Química, Universitat de Barcelona, Martí I Franquès 1-11, Barcelona, CP, 08028, Spain
[b] Departamento de Química, División de Ciencias Naturales y Exactas, Universidad de Guanajuato, Cerro de la Venada s/n, Pueblito de Rocha, 36040, Guanajuato, Mexico

HIGHLIGHTS

- Innovative advances of the PEF process in the period 2019–2023 are summarized.
- Similar degradation of organic pollutants with homogeneous EF, PEF, and SPEF at pH 3.0
- Larger mineralization by SPEF than PEF due to the greater UV intensity of sunlight.
- Excellent performance of heterogeneous PEF with a MOFs (2Fe/Co)/carbon fiber cathode at pH 3.0
- Novel hybrid methods with photo(electro)catalysis and sequential with electrocoagulation or persulfate.

GRAPHICAL ABSTRACT

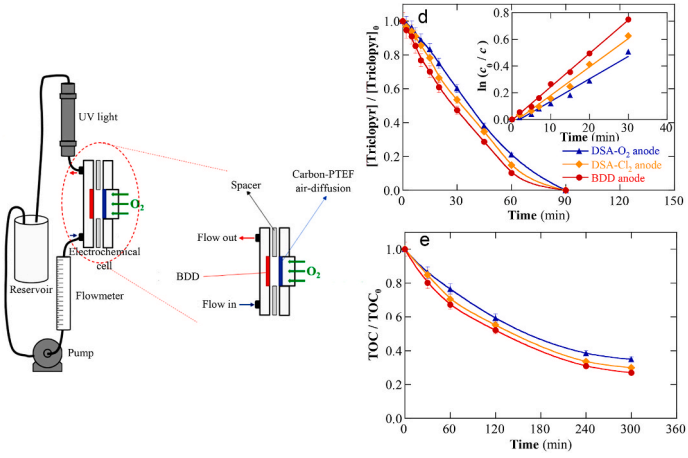

ARTICLE INFO

Handling editor: Y Yeomin Yoon

Keywords:
Homogeneous photoelectro-Fenton
Homogeneous solar photoelectro-Fenton
Heterogeneous photoelectro-Fenton
Photoelectro-fenton/photoelectrocatalysis
Electrocoagulation-photoelectro-Fenton
Water treatment

ABSTRACT

Wastewaters with toxic and recalcitrant organic contaminants are poorly remediated in conventional wastewater treatment plants. So, powerful processes need to be developed to destroy such organic pollutants to preserve the quality of the aquatic environment. This critical and comprehensive review presents the recent innovative development of photoelectro-Fenton (PEF) covering the period 2019–September 2024. This emerging photo-assisted Fenton-based electrochemical advanced oxidation process (EAOP) is an efficient and cost-effective treatment for water remediation. It possesses a great oxidation power because the *in-situ* generated hydroxyl radical as oxidant is combined with the photolysis of the organic by-products under UV or sunlight irradiation. The review is initiated by a brief description of the characteristics of the PEF process to stand out in the role of generated oxidizing agents. Further, the homogeneous PEF. PEF-like, solar PEF (SPEF), and SPEF-like processes with iron catalysts are discussed, taking examples of their application to the removal and mineralization of solutions of industrial chemicals, herbicides, dyes, pharmaceuticals, and direct real wastewaters. Novel

* Corresponding author.
** Corresponding author.
E-mail addresses: brillas@ub.edu (E. Brillas), juan.peralta@ugto.mx (J.M. Peralta-Hernandez).

https://doi.org/10.1016/j.chemosphere.2024.143465
Received 31 July 2024; Received in revised form 2 October 2024; Accepted 2 October 2024
Available online 5 October 2024

heterogeneous PEF treatments of such pollutants with solid iron catalysts or functionalized cathodes are analyzed. Finally, novel hybrid processes including PEF/photocatalysis and PEF/photoelectrocatalysis, followed by novel and potent sequential processes like electrocoagulation-PEF and persulfate-PEF, are discussed. Throughout the manuscript, special attention was made to the total operating cost of PEF, which is more expensive than conventional electro-Fenton due to the high electric cost of the UV lamp, pointing to consider the much more cost-effective SPEF as a preferable alternative in practice.

1. Introduction

The accumulation of organic and inorganic pollutants into water bodies worldwide from wastewater causes a continuous loss of water quality for the subsistence and consumption of animals and humans. Many industrial chemicals, herbicides, dyes, and drugs in wastewater are released daily into natural waters (Brillas, 2020; Sirés and Brillas, 2021). Persistent organic pollutants (POPs) are inefficiently removed in municipal wastewater treatment plants (WWTPs) by traditional physicochemical and biological processes. Since they are largely stable to ambient conditions and solar light, their accumulation is favored in lakes, rivers, and oceans, and even in drinking water, at levels from ng L^{-1} to μg L^{-1} (Martínez-Huitle and Brillas, 2021; Pacheco-Álvarez et al., 2022). Most POPs in the aquatic environment are toxic and can originate hazardous health effects on living beings. This makes necessary the proposal and development of simple, safe, and effective powerful oxidation technologies to ensure their removal from water.

Over the last decades, advanced oxidation processes (AOPs) including chemical, photochemical, electrochemical, and photoelectrochemical techniques have been developed for the remediation of wastewaters containing POPs (Brillas and Garcia-Segura, 2023; Brillas and Peralta-Hernández, 2023). AOPs are based on the *in-situ* generation of reactive oxygen species (ROS) like hydroxyl radical ($^{\bullet}$OH) that can attack organics up to their mineralization, the reason for which are considered environmentally friendly methods. The large oxidation ability of $^{\bullet}$OH over most organic pollutants is due to its high standard reduction potential (E°) of 2.80 V/SHE) (Nidheesh et al., 2018). The most ubiquitous chemical AOP is the Fenton method which consists of the addition of a mixture of Fe^{2+} and H_2O_2, the so-called Fenton's reagent, which originates homogeneous $^{\bullet}$OH by the classical Fenton's reaction (Deng et al., 2023). However, the mineralization of organic pollutants in this technique is impeded by the formation of Fe(III) complexes with final short-linear aliphatic carboxylic acids, hardly oxidizable by $^{\bullet}$OH. The photo-Fenton (PF) or solar PF (SPF) techniques, overcome this problem because the solution is illuminated by UV light or sunlight producing more $^{\bullet}$OH with photolysis of the Fe(III) complexes formed, thus significantly enhancing its mineralization process (Brillas, 2020).

Electrochemical AOPs (EAOPs) are of great technological interest because they are environmentally compatible operating at mild conditions with versatility, high efficiency, safety, and amenability of automation (Nidheesh et al., 2018; Poza-Nogueiras et al., 2018). Electro-Fenton (EF) as the ubiquitous Fenton-based EAOP is more powerful than the Fenton method. In EF, both reagents (Fe^{2+} and H_2O_2) are produced in an electrolytic cell and organics can be destroyed by homogeneous $^{\bullet}$OH generated from Fenton's reaction, by direct anodic oxidation, and/or mediated oxidation with heterogeneous $^{\bullet}$OH formed from water discharge at the anode (Poza-Nogueiras et al., 2018). Then, it outperforms the simpler anodic oxidation (AO) process where organic pollutants are only removed by direct or mediated oxidation at the anode of the electrolytic cell (Sirés and Brillas, 2021). In many cases, EF shows weak mineralization as a result of the ineffective attack of homogeneous and heterogeneous $^{\bullet}$OH on the recalcitrant final Fe (III)-carboxylate complexes generated (Deng et al., 2023). Like in the case of the photo-Fenton method, the exposition of the treated EF solution to UV light upgrades the mineralization efficiency in the photoelectro-Fenton (PEF) process. The alternative use of sunlight as an inexpensive and renewable source of light energy allows the application of the solar PEF (SPEF) process that usually improves the PEF by the higher irradiance of sunlight with respect to conventional UV lamps.

In previous work, one of us published a comprehensive review of the application of PEF processes to the removal of waters contaminated with POPs (Brillas, 2020). It summarized the articles reported from 2010 to 2018, also covering those with data from 2019 in the last year. Since no further reviews have been published in the literature on this interesting issue, we have undertaken a review of the articles reported on it in the period 2019–September 2024, without considering those published in 2018 with data in 2019. A search in the Scopus database with the keywords "Photoelectro-Fenton" and "organic pollutants" allowed the selection of 85 scientific papers showing innovative PEF treatments for organics in this period.

This paper presents a critical and comprehensive review of the main innovative applications of PEF and related processes for synthetic and real wastewater remediation shown in the above articles. First, the characteristics operating variables, and parameters of PEF and SPEF are briefly described to discuss their oxidation ability and the role of produced oxidants and irradiated UV or solar light. Further, the abatement of industrial chemicals, herbicides, dyes, and drugs in synthetic solutions and real wastewater is summarized by homogeneous PEF, PEF-like, SPEF, and SPEF-like processes. While Fe^{2+} acts over electrogenerated H_2O_2 in PEF and SPEF, their like processes stabilize this ion by quenchers or use HClO instead of H_2O_2. After this, heterogeneous PEF methods with solid catalysts or functionalized cathodes are detailed. The final part analyzes combined treatments, coupling hybrid PEF with photocatalysis (PC) and photoelectrocatalysis (PEC), and sequential electrocoagulation (EC) or persulfate (PS) with PEF.

2. Characteristics of the photoelectro-Fenton process

PEF involves the 2-electron reduction at the cathode of injected O_2 to yield H_2O_2 by reaction (1) in an acidic medium with $E^{\circ} = +0.68$ V/SHE (Deng et al., 2023). A 3D cathode like a gas-diffusion electrode (GDE) directly fed with O_2 or air or a 2D cathode fed with dissolved O_2 in the solution can be used. Reaction (1) competes with the cathodic reduction of H^+ to H_2 with $E^{\circ} = 0$ V/SHE, also being easier than the cathodic 4-electron reduction of O_2 to H_2O with $E^{\circ} = +1.23$ V/SHE. 3D and 2D carbonaceous cathodes yield the best efficiency for H_2O_2 electrogeneration from reaction (1). Nevertheless, when an undivided cell is used, the accumulated H_2O_2 is oxidized at the anode M giving the weaker oxidant hydroperoxyl radical ($M(HO_2^{\bullet})$) by reaction (2) (Sirés and Brillas, 2021). This reaction competes with the anodic water oxidation leading to the heterogeneous $M(^{\bullet}OH)$ by reaction (3), limited to the anode surface. At high current, O_3 can be generated from reaction (4) (Brillas, 2020)

$$O_2 + 2H^+ + 2e^- \rightarrow H_2O_2 \quad (1)$$

$$M + H_2O_2 \rightarrow M(HO_2^{\bullet}) + H^+ + e^- \quad (2)$$

$$M + H_2O \rightarrow M(^{\bullet}OH) + H^+ + e^- \quad (3)$$

$$3H_2O \rightarrow O_3 + 6H^+ + 6e^- \quad (4)$$

When AO is performed with electrogenerated H_2O_2, it corresponds to the AO-H_2O_2 process. The AO process is slightly less potent than the AO-H_2O_2 one due to the very low oxidation power of H_2O_2, being the

generated oxidant M(•OH) from reaction (3) the main oxidant in both cases. Note that the oxidation ability of both methods is a function of the anode used. Boron-doped diamond (BDD) thin-film electrodes have been found the most preferable in non-chloride media since they produce more amount of reactive BDD(•OH) than M(•OH) from conventional Pt or dimensionally stable anodes (DSA) based on RuO_2 and/or IrO_2 (Brillas, 2020; Sirés and Brillas, 20212). The anode also presents a notable effect in the EF process, but it is much less significant in PEF and SPEF because of the fast organic removal by the incident photons.

The homogeneous EF process strongly upgrades the oxidation power of the electrogenerated H_2O_2 by adding a small quantity of Fe^{2+} as the catalyst that originates homogeneous •OH from the well-known Fenton's reaction (5) at optimum pH near 3 (Sirés and Brillas, 2021):

$$Fe^{2+} + H_2O_2 \rightarrow Fe^{3+} + {}^{\bullet}OH + OH^- \; k_2 = 63\ M^{-1}\ s^{-1} \quad (5)$$

This process yields a variety of ROS including not only •OH but also $HO_2^{\bullet}$ and superoxide radical anion ($O_2^{\bullet-}$), whose reactions are specified in Table SM-1 of Supplementary Material in the previous work of Brillas (2020).

The advantages of the homogeneous EF process over chemical Fenton are: (i) the *in-situ* H_2O_2 electrogenerated in EF avoids being transported and handled as needed in chemical Fenton, which is dangerous because of its explosive thermal decomposition, and (ii) a small quantity of Fe^{2+} (usually ≤0.5 mM) is needed in EF because Fe^{2+} can be continuously regenerated from the cathodic reduction of Fe^{3+} by reaction (6) with $E^\circ = +0.77$ V/SHE, thus maintaining the •OH generation in the catalytic Fe^{3+}/Fe^{2+} loop (Deng et al., 2023). This differs from chemical Fenton where a stoichiometric molar H_2O_2/Fe^{2+} ratio is used for an efficient •OH generation giving rise to a much higher amount of recyclable iron hydroxide sludge and making a much more expensive process.

$$Fe^{3+} + e^- \rightarrow Fe^{2+} \quad (6)$$

In the homogeneous EF treatment, organic pollutants are attacked preeminently by homogeneous •OH and heterogeneous M(•OH), although it possesses the following drawbacks: (i) its better performance occurs in an acidic medium, usually it is optimal at pH 3 rapidly losing efficiency at pH > 4 due to the precipitation of iron hydroxides and (ii) the formation of recalcitrant Fe(III) complexes with intermediates like final Fe (III)-carboxylate species largely inhibits the mineralization process (Brillas and Garcia-Segura, 2023). The use of PEF treatments can solve these problems.

Several artificial lamps are used as irradiation sourced in PEF. They can emit UVC light with λ = 100–280 nm, UVB light with λ = 280–315 nm, or UVA lamp with λ = 315–400 nm (Brillas, 2020). These irradiations enhance the rate of Fenton's reaction (5) since they originate extra Fe^{2+} regeneration by: (i) $Fe(OH)^{2+}$ photoreduction pre-eminently at pH 2.8–3.5, with additional •OH production, by photo-Fenton reaction (7) and (ii) photolysis of Fe(III)-carboxylate species following the general reaction (8). Furthermore, by applying a UVC light, organic pollutants can also be photolyzed and H_2O_2 undergoes homolytic decomposition to extra homogeneous •OH by reaction (9).

$$Fe(OH)^{2+} + h\nu \rightarrow Fe^{2+} + {}^{\bullet}OH \quad (7)$$

$$Fe(OOCR)^{2+} + h\nu \rightarrow Fe^{2+} + CO_2 + R^{\bullet} \quad (8)$$

$$H_2O_2 + h\nu \rightarrow 2{}^{\bullet}OH \quad (9)$$

The high electrical cost of the artificial UV lamp represents a drawback for the application of the homogeneous PEF treatment at an industrial scale. This is overcome using the much more cost-effective homogeneous SPEF method where the solution is irradiated with sunlight, of λ > 300 nm, also showing greater degradation and mineralization rates of organics with respect to PEF by (i) its high UV input and (ii) additional photolysis at λ > 400 nm, that enhances the photodecarboxylation of Fe(III)-carboxylate complexes by reaction (8) (Brillas, 2020). However, the main restriction of the homogeneous SPEF process is that it can only be applied to the daily hours of sun, depending on the climatology and geographic site.

Heterogeneous PEF processes have been proposed with two strategies, using solid (insoluble) catalysts or functionalized cathodic materials. Iron is usually employed in the catalyst in both cases, which possesses surface Fe^{2+}, denoted as ≡ Fe^{2+} typically linked to –OH groups. This species yields the heterogeneous Fenton's reaction (10) with a production of surface ≡ Fe^{3+} and heterogeneous •OH from electrogenerated H_2O_2, similarly to the homogeneous Fenton's reaction (5). Reaction (10) makes feasible the extension of heterogeneous •OH to pH near 7, favoring the low dissolution of iron ions and increasing the catalyst reusability preventing sludge formation.

$$\equiv Fe^{2+} + H_2O_2 \rightarrow \equiv Fe^{3+} + {}^{\bullet}OH + OH^- \quad (10)$$

SO_4^{2-} and Cl^- anions present in real wastewater can also be oxidized at the anode of an undivided cell originating other oxidants of organics. So, SO_4^{2-} can be transformed into the weak oxidant persulfate ($S_2O_8^{2-}$) ion via reaction (11), which can be activated to form the strong oxidant sulfate radical anion ($SO_4^{\bullet-}$) with an E° value between +2.5 and + 3.1 V/SHE depending on pH (Brillas and Peralta-Hernández, 2023). On the other hand, it is well-known that Cl^- can be transformed into several active chlorine species as function of pH by reactions (12)–(14), namely Cl_2 ($E^\circ = +1.36$ V/SHE) at pH < 3, HClO ($E^\circ = +1.49$ V/SHE) at pH 3–8, and ClO^- ($E^\circ = +0.89$ V/SHE) at pH > 8 (Brillas and Garcia-Segura, 2023). These active chlorine species can oxidize organics producing toxic chloroderivatives, alongside ClO_3^- and ClO_4^- ions that persist after treatment. The viability of the applied process then needs to be monitored by measuring the extent of such by-products.

$$2SO_4^{2-} \rightarrow S_2O_8^{2-} + 2e^- \quad (11)$$

$$2Cl^- \rightarrow Cl_2 + 2e^- \quad (12)$$

$$Cl_2 + H_2O \rightarrow HClO + Cl^- + H^+ \quad (13)$$

$$HClO \leftarrow ClO^- + H^+ \; pK_a = 7.54 \quad (14)$$

Apart from the generation of oxidants, it is also noticeable that SO_4^{2-} and Cl^- anions partially quench the Fe^{2+} cations present in the solution diminishing its content ascatalyst for Fenton's reaction (5) and photo-Fenton reaction (7). The concentration of both anions is then an important parameter to be considered in the photo-assisted Fenton-based EAOPs Other anions can influence the performance of the treatments. While NO_3^- is an inert species that does not form complexes with Fe^{2+}, the phosphate ions are strong quenchers that largely inhibit the PEF and SPEF processes.

3. Operating variables and parameters

The performance of photo-assisted Fenton-based EAOPs relies on some operating variables like catalyst and pollutant concentrations, electrolyte composition, solution stirring and pH, applied current (*I*) or current density (*j*), nature of the electrodes, cell configuration, and incident radiation. They affect the evolution of experimental parameters like: (i) the absorbance (*A*) of a dye at the λ_{max} of its UV/Vis spectrum, (ii) the concentration (*c*) of the target molecule measured by reversed-phase high-performance liquid chromatography (HPLC), and (iii) the chemical oxygen demand (COD) and total organic carbon (TOC) of the solution to monitor the abatement of oxidizable products and the mineralization process, respectively. In some articles, primary intermediates and final short-linear carboxylic acids can be identified by gas chromatography/mass spectrometry (GC/MS), liquid mass coupled to MS (LC-MS), and ion-exclusion HPLC. The detection of these species allows proposing a degradation or mineralization route for the target molecule. Moreover, released inorganic ions can be identified by chromatographic or colorimetric methods. In some cases, the drastic loss of

acute toxicity is determined to show the feasibility of a biological post-treatment before disposal.

Figures-of-merit present the parameters in front of electrolysis time (t, in s, min, h, or d) or specific charge consumed (Q, in Ah L^{-1}). Normalized parameters correspond to the X/X_0 ratio, where X_0 and X are the initial and at a given t or Q value. Namely, A, c (in mg L^{-1}), COD (in mg O_2 L^{-1}), and TOC (in mg C L^{-1}). It is also very usual to give the percentage of parameter removal, according to the general Eq. (15) (Brillas, 2020):

$$\%\,X = \frac{X_0 - X}{X_0}\,100 \tag{15}$$

For A measurement, this term is known as the percentage of color removal or discoloration efficiency.

The plots of the decay of ln (A_0/A), ln (c_0/c), or ln (TOC_0/TOC) vs. time are usually straight lines obeying a pseudo-first-order kinetics. This behavior indicates that the discoloration, degradation, or mineralization process is limited by the quantity of ROS (pre-eminently $^{\bullet}OH$) *in-situ* produced in the electrolytic system. The slope of such linear relations is denoted as k_{dis}, k_1, or k_{TOC}, known as pseudo-first-order rate constant for discoloration, target compound decay, or TOC removal. The latter constant in much slower than the two former ones because the formed by-products are destroyed much more slowly than the initial contaminant.

The change of TOC with time allows the calculation of the mineralization current efficiency (MCE, in %) at a given time t (in s) as follows (Brillas, 2020):

$$\%\,MCE = \frac{n\,F\,V\,\triangle TOC}{4.32\times10^7\,m\,I\,t}\,100 \tag{16}$$

Where n denotes the theoretical number of electrons consumed in the mineralization, F is the Faraday constant (96,485 C mol^{-1}), V is the solution volume (in L), $\triangle$TOC is the loss of TOC content (in mg C L^{-1}), 4.32×10^7 is a conversion factor (=3600 s h^{-1} × 12,000 mg C mol^{-1}), m is the number of carbon atoms of the target molecule, and I is the applied current (in A). Similarly, the average current efficiency (ACE, in %) can be determined from Eq, (17):

$$\%\,ACE = \frac{F\,V\,\triangle COD}{8\,I\,t}\,100 \tag{17}$$

where $\triangle$COD is the COD decay (in g O_2 L^{-1}), 8 is the oxygen equivalent mass (in g eq^{-1}), and the other magnitudes are the same as Eq. (15).

Some energetics parameters related to the electrical consumption of the process are also calculated. The energy consumption per unit volume (EC, in kWh m^{-3}) is determined by Eq. (18), whereas the energy consumption per g of TOC (EC_{TOC}, in kWh (g TOC)$^{-1}$) or per g of COD (EC_{COD}, in kWh (g COD)$^{-1}$) is obtained by the general Eq. (19) (Brillas and Garcia-Segura, 2023):

$$EC\ (kWh\ m^{-3}) = \frac{E_{cell}\,I\,t}{V} \tag{18}$$

$$EC_x\ (kWh\ (kg\ X)^{-1}) = \frac{E_{cell}\,I\,t}{V\,\triangle X} \tag{19}$$

where E_{cell} is the average cell voltage (in V) and t is the electrolysis time (in h). In PEF processes, the high energy consumption related to the UV lamp is not usually considered in such equations because they acquire too high values. Many cost-performance evaluations and techno-economic studies are required in the future to assess such treatments.

4. Homogeneous photoelectro-Fenton process

The homogeneous PEF process is the most common photo-assisted Fenton-based EAOP for removing organic pollutants from wastewater. Key operating variables are the cell configuration and electrodes, which determine the H_2O_2 electrogenerated and Fe^{2+} regeneration for $^{\bullet}OH$ production via Fenton's reaction (5). The process is carried out in batches for a long time aiming to achieve the maximum mineralization, once reached, if possible, overall degradation. Undivided two-electrode cells are used, and in minor proportion three-electrode cells, operating under galvanostatic or potentiostatic mode, respectively. Short inter-electrode gaps <2 cm are selected for attaining a low ohmic drop with the consequent energy saving. An inner or external UV lamp is applied to illuminate the solution.

Fig. 1 schematizes several experimental setups used for PEF with two-electrode cells in batch. In some cases, the cell possessed a jacket with water recirculation to maintain a given temperature in the solution. Fig. 1a exemplifies the ubiquitous configuration of a stirred tank reactor with an external UVA light above the solution (Brillas, 2020). In the flow system of Fig. 1b, the cell is a stirred tank reactor equipped with electrodes, recirculating the solution through an external UV photoreactor at a liquid flow rate regulated by a flowmeter or rotameter/(Brillas, 2020). This system differs from the typical flow system of Fig. 1c in which the solution contained in a reservoir is injected into a flow-by-filter-press electrochemical reactor with parallel electrodes to subsequently pass through a UV photoreactor (Da Costa et al., 2021). Fig. 1d shows a flow-through filter-press electrochemical reactor with the solution passing through both electrodes and Fig. 1e, the corresponding flow system with an external UV light directly illuminating the solution contained in the reservoir (Cornejo et al., 2023b).

Table 1 collects the main results obtained for homogeneous PEF, PEF-like, SPEF, and SPEF-like processes of selected industrial chemicals, herbicides, dyes, drugs, and real wastewater. A look at this table confirms that most works consider the use of a BDD anode in synthetic sulfate medium by its superior oxidation power with respect to DSA ones, which were explored in chloride media Moreover, it can be observed that 3D GDE of carbon-PTFE O_2- or air-diffusion, without or with modification, were the most popular cathodes, followed by 2D cathodes such as carbon felt, graphite, or BDD. The advantage of using GDE cathodes (see an example in Fig. 1a) is the much higher H_2O_2 accumulation provided to the medium with respect to the 2D ones (Brillas, 2020). Although this behavior presupposes an initial faster rate for Fenton's reaction (5), their high selectivity on O_2 reduction from reaction (1) inhibits the Fe^{2+} regeneration from reaction (6), decreasing the efficiency of $^{\bullet}OH$ production by Fenton's reaction (5) and favoring the formation of recalcitrant Fe(III)-carboxylate complexes. The incident light in PEF then results crucial to drastically photolyze such complexes, thus enhancing the mineralization of the target molecule. In contrast, the 2D cathodes with much smaller H_2O_2 electrogeneration become much more effective for Fe^{2+} regeneration from reaction (6), maintaining a more constant $^{\bullet}OH$ production by Fenton's reaction (5) and generating less amount of hardly oxidizable final Fe(III)-carboxylate species. In this section, the application of the different anode/cathode systems for the removal of organic pollutants by homogeneous PEF is summarized and discussed.

4.1. Industrial chemicals

Homogeneous PEF has been applied to the removal of several industrial chemicals in waters. 4-Aminoantipyrine (da Silva et al., 2019), bentothiazoles (Xu et al., 2019), formic and oxalic acids (Ma et al., 2021), methylparaben (Fortunato et al., 2020; dos Santos et al., 2021; Barazorda-Ccahuana et al., 2023), and phenol (An et al., 2020; Mousset et al., 2021), have been examined. The data in Table 1 indicate that such processes were performed with a BDD anode and a GDE cathode with 0.050 M Na_2SO_4 at pH 2.5–3.0. Among the operating variables checked, was found a decay in the degradation rate with increasing the target pollutant content by the slower destruction of greater organic load with a similar production of homogeneous and heterogeneous $^{\bullet}OH$. On the other hand, limit values of Fe^{2+} content and j are achieved because greater values of both variables cause a decay of the relative amount of

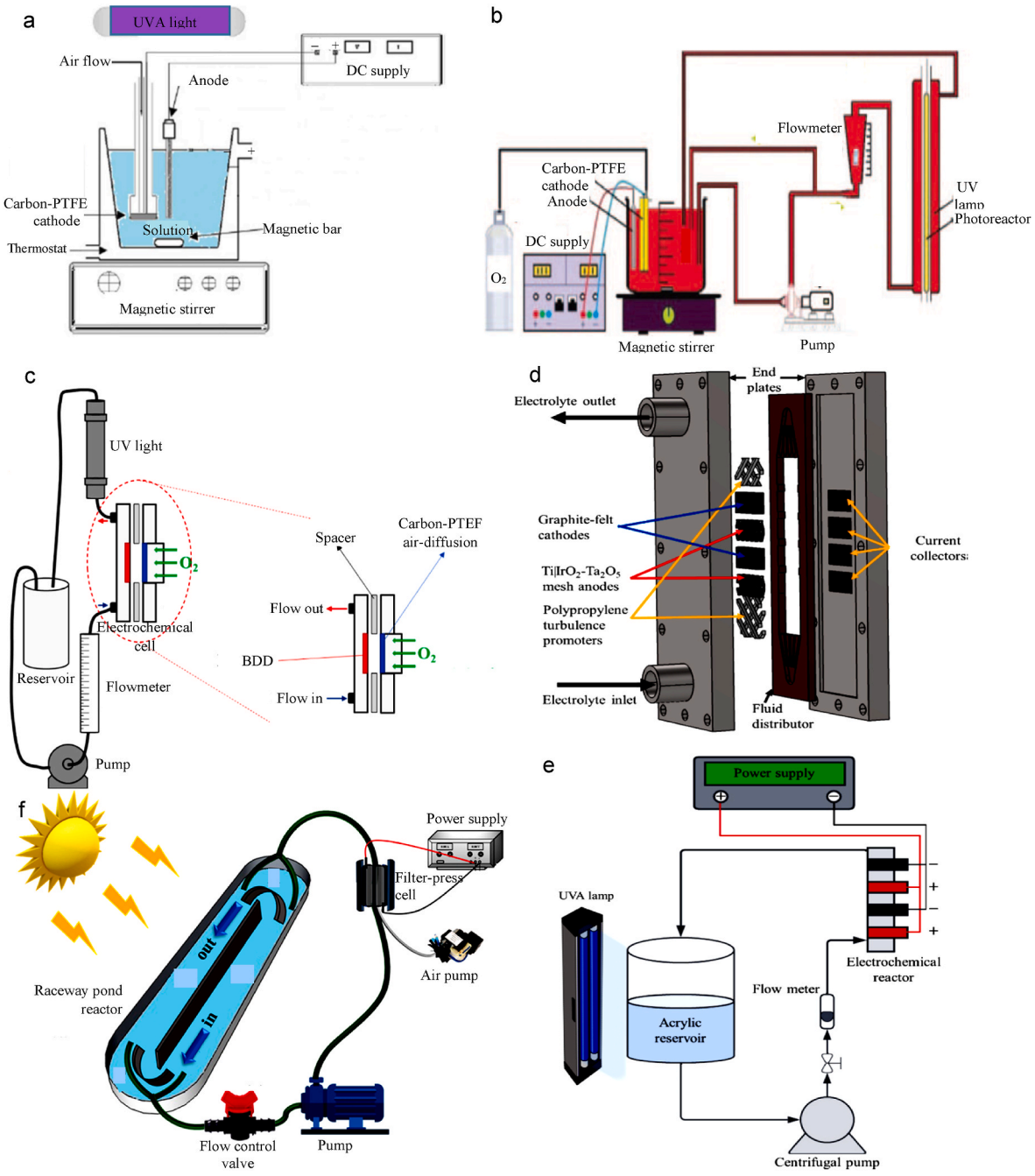

Fig. 1. Scheme of experimental setups used for the homogeneous (a–e) PEF and (f) SPEF treatments of organic pollutants in wastewaters with two-electrode cells in batch. (a) Stirred tank reactor with a carbon-PTFE cathode and a UVA lamp above the solution (adapted from Brillas (2020)). (b) Flow plant with a stirred tank reactor and external UV light (adapted from Brillas (2020)). (c) Flow-by filter-press cell connected to a UV light compartment (adapted from Da Costa et al. (2021)). (d) Flow-through filter-press cell and (e) lab-scale flow system under UVA light (adapted from Cornejo et al. (2023b)). (e) Flow raceway pond reactor upon sunlight connected to a single filter-press cell (adapted from Campos et al. (2023)).

generated •OH by the larger acceleration of its non-oxidizing parasitic reactions (Brillas and Garcia-Segura, 2023; Brillas and Peralta-Hernández, 2023), thus inhibiting the degradation and mineralization of the target molecule. These trends are verified for all the PEF ′and SPEF processes.

The work of da Silva et al. (2019) optimized the removal of 4-aminoantipyrine in pure water using response surface methodology and found that this chemical underwent a 99% removal in 7 min for 62.5 mg L^{-1} with 47.75 mg L^{-1} Fe^{2+}, j = 77.5 mA cm^{-2}, and 4 W UVA light (see Table 1). The prolongation of the electrolysis to 170 min only yielded 64% of mineralization. It is noticeable that similar results were determined in a WWTP effluent, although a slower process should be expected by the consumption of •OH with the organic pollutants and inorganic ions of the WWTP. For 0.5 mM methylparaben in pure water, Fortunato et al. (2020) reported that the degradation and TOC decays grew in the order: of AO-H_2O_2 < AO-H_2O_2/UVC ≤ EF < PEF. The PEF process was more powerful than in the above article because a more portent 5 W UVC light was applied and thus, total removal and 91% TOC abatement with 21% MCE were determined for 0.5 mM Fe^{2+} and j = 33.3 mA cm^{-2} lasting 180 min (see Table 1). Moreover, these authors identified 3 aromatic intermediates and oxalic acid by GC/MS and HPLC. Similar excellent results have been described by

Table 1
Selected results were reported for homogeneous photoelectro-Fenton (PEF), PEF-like, solar PEF (SPEF), and SPEF-like treatments of aqueous matrices contaminated with organic pollutants by different electrochemical systems.

System (anode, cathode)	Pollutant	Experimental remarks	Best results	Ref.
Homogeneous PEF rowhead				
Industrial chemicals rowhead				
Like Fig. 1a (BDD [a], carbon-PTFE air-diffusion)	4-Aminoantipyrine	100 mL of 25–175 mg L^{-1} chemical in pure water and secondary WWTP effluent, 0.050 M Na_2SO_4, 2–63 mg L^{-1} Fe^{2+}, pH = 3.0, 25 °C, j [b] = 10–100 mA cm^{-2}, 4 W UVA light, 170 min	In pure water, optimized by response surface methodology: 99% removal for 62.5 mg L^{-1} chemical with 47.75 mg L^{-1} Fe^{2+} and j = 77.5 mA cm^{-2} at 7 min. 64% mineralization at 170 min. Similar results with the WWTP effluent	da Silva et al. (2019)
Like Fig. 1a (BDD, Pd/carbon-PTFE O_2-diffusion)	Methylparaben	150 mL of 0.5 mM chemical in pure water, 0.050 M Na_2SO_4, 0.1–0.5 mM Fe^{2+}, pH = 2.5, 25 °C, j = 33.3 mA cm^{-2}, 5 W UVC light, 180 min	Degradation and TOC decay: AO-H_2O_2 < AO-H_2O_2/UVC ≤ EF < PEF (total removal, 91% TOC decay, and 21% MCE). 3 aromatics and oxalic acid found by GC/MS and HPLC	Fortunato et al. (2020)
Like Fig. 1c (BDD, polyacrylonitrile-carbon fiber air-diffusion)	Phenol	600 mL of 1.4 mM chemical in pure water, 0.050 M K_2SO_4, 0.05–0.2 mM Fe^{2+}, pH = 3.0, room temperature, j = 0.625–2.5 mA cm^{-2}, liquid flow rate = 0.4 L min^{-1}, 12 W UVC light, 160 min	Determination of overall cost and percent of cost distribution for ozonation, Fenton, PF, EF, and PEF. EF was the cheaper process with 125 € m^{-3} (g TOC)$^{-1}$ for 99% of mineralization.	Mousset et al. (2021)
Like Fig. 1a (BDD, carbon-PTFE O_2-diffusion	Methylparaben	150 mL of 0.5 mM chemical in pure water, 0.050 M Na_2SO_4, 0.5 mM Fe^{2+}, pH = 3.0, 25 °C, j = 16.6 mA cm^{-2}, 5.8 and 14.8 mW cm^{-2} UVA and UVC lights, respectively, 180 min	Total removal: 20 min by PEF-UVC ($k_1 = 3.9 \times 10^{-3}$ s^{-1}) and 30 min for PEF-UVA and EF ($k_1 = 2.7 \times 10^{-3}$ s^{-1}). Total mineralization for both PEF with near 40% MCE. Detected 3 aromatics and 4 carboxylic acids by GC/MS	Barazorda-Ccahuana et al. (2023)
Herbicides rowhead				
Like Fig. 1c (BDD, MoSP/MWCNTs [c] air-diffusion)	Bentazon	2.5 L of 20 mg L^{-1} herbicide in pure water, 0.050 M Na_2SO_4, 0.5 mM Fe^{2+}, pH = 3.0, 35 °C, j = 25 mA cm^{-2}, liquid flow rate = 180 L h^{-1}, 160 W UVA light, 240 min	Overall degradation in 20 min with $k_1 = 0.1875$ min^{-1} and 77% TOC decay in 240 min with 12% MCE. Detection of released SO_4^{2-}, NO_3^-, and NH_4^+	Alcaide et al. (2020)
Fig. 1c (BDD, carbon-PTFE O_2-diffusion)	Tebuthiuron	2 L of 100 mg L^{-1} herbicide in pure water, 0.1 M K_2SO_4, 0.5 mM Fe^{2+}, pH = 3.0, 25 °C, j = 75 mA cm^{-2}, liquid flow rate = 50 L h^{-1}, 64 W m^{-2} UVC light, 360 min	95% removal in 120 min ($k_1 = 3.2 \times 10^{-4}$ s^{-1}) and 92% TOC decay in 360 min k_1: 5.9×10^{-5} s^{-1} for EF < 2.6×10^{-4} s^{-1} for AO-H_2O_2/UVC. Detection of released NO_3^-, NO_2^-, ClO_2^-, and ClO_3^-	Da Costa et al. (2021)
Stirred tank reactor upon external light (Ti/$Ru_{0.3}Ti_{0.7}O_2$ electrodes, H_2O_2 addition)	Glyphosate	100 mL of 100 mg L^{-1} herbicide in pure water, 0.050 M Na_2SO_4, 10 mg L^{-1} Fe^{2+}, 100 mg L^{-1} H_2O_2, pH = 3.0, room temperature, j = 50 mA cm^{-2}, 6 W UVC light, 120 min	Degradation, COD removal, and TOC decay: 70%, 82%, and 79% for EF-Fered <74%, 86%, and 85% for PEF-Fered	da Silva et al. (2022)
Dyes rowhead				
Like Fig. 1a (Ti/$Ru_{0.15}Ti_{0.85}O_2$, carbon-PTFE air-diffusion)	Reactive Blue 4	150 mL of 36.2 mM dye in pure water, 0.050 M Na_2SO_4 or 0.15 M NaCl, 0.5 mM Fe^{2+}, pH = 3.0, 35 °C, I [d] = 100 and 200 mA, 12 W UVA light, 360 min	94% color removal in 30 min by PEF with 0.15 M NaCl and 70 min by EF and PEF with 0.050 M Na_2SO_4. Under the last conditions, TOC removal: 33% by EF < 70% by PEF	Nakamura et al. (2019)
Stirred tank reactor (BDD, carbon felt, injected air)	Erythrosine B	300 mL of 100 mg L^{-1} dye in pure water, 0.050 M Na_2SO_4, 0.1 mM Fe^{2+}, pH = 3.0, room temperature, j = 20 mA cm^{-2}, 25 and 100 W UVA lights, 120 min	Overall discoloration: SPEF = PEF-100 W UVA (20 min) < PEF-25 W UVA (35 min) < EF (50 min). COD removal: 100% SPEF, PEF-100 W UVA (90 min) > 97% PEF-25 W UVA (120 min) > 91% EF (120 min)	Clematis and Panizza (2021)
Stirred tank reactor (BDD, carbon felt, injected air)	Direct Red 23	230 mL of 80 mg L^{-1} dye in pure water, 0.050 M Na_2SO_4 and 0.10 M NaCl, 0.1 mM Fe^{2+}, pH = 3.0, 20 °C, j = 2.5–15 mA cm^{-2}, UVA LED light (λ = 400 nm), 360 min	Increasing discoloration at higher j. Faster loss of color with NaCl. Conversely, for j = 5 mA cm^{-2}, TOC decay: 59% for AO-H_2O_2 < 63% photo- AO-H_2O_2 < 68% for EF < 76% for PEF using NaCl, lower than 82% for AO-H_2O_2 < 87% photo- AO-H_2O_2 < 90% for EF < 95% for PEF using Na_2SO_4	Titchou et al. (2022)
Stirred tank reactor (BDD, BDD, injected air)	Brown HT	160 mL of 50 and 80 mg L^{-1} dye in pure water, 0.050 M Na_2SO_4, 0.5 mM Fe^{2+}, pH = 3.0, room temperature, j = 71 mA cm^{-2}, 75 mW cm^{-2} UVA light, 60 min	100% discoloration with k_{dis} = 0.120 and 0.085 min^{-1} for 50 and 80 mg L^{-1} dye by EF and PEF. For PEF: 80% COD removal. Evolution of generated glyoxylic, oxalic, and oxamic acids by HPLC	Corona-Bautista et al. (2021)
Drugs rowhead				
Like Fig. 1a (Ti/RuO_2, agarose-derived carbon-PTFE air-diffusion)	Acebutolol	150 mL of 0.046 mM drug (10 mg L^{-1} TOC_0) in pure water and WWTP effluent (10.4 mg L^{-1} TOC_0), 0.05 M Na_2SO_4, 0.5 mM Fe^{2+}, pH = 3.0, 25 °C, j = 60 mA cm^{-2}, 6 W UVA light, 360 min	Complete removal in 9 min with $k_1 = 0.477$ min^{-1} and 90% TOC abatement in 360 min. Using the WWTP effluent, total degradation in 60 min and 47% TOC decay in 360 min	Zhang et al. (2022)
Like Fig. 1a (BDD, carbon-PTFE air-diffusion onto several substrates)	Carbenicillin	150 mL of 0.049 mM drug in simulated and WWTP effluents, 0.010 M Na_2SO_4, 0.50 mM Fe^{2+}, pH = 3.0, 25 °C, I = 20 mA, 6 W UVA light, 480 min	Overall degradation in 13 min for Na_2SO_4, 15 min for simulated, and 18 min for WWTP. TOC decay: 95%, 67%, and 80% in 480 min in such media. 23 aromatic by-products, 7 aliphatic derivatives, and 7 carboxylic acids detected by HPLC	Ren et al. (2023)
Like Fig. 1a (BDD, modified carbon-PTFE O_2-diffusion with 1,4-naphthoquinone)	Paracetamol	450 mL of 180 mg L^{-1} drug in pure water, 0.1 M K_2SO_4, 0.15 mM Fe^{2+}, pH = 2.0, 20 °C, j = 75 mA cm^{-2}, UVC light, 180 min	Degradation: 74–76% with $k_1 = 0.0082$ min^{-1} for AO-H_2O_2 and AO-H_2O_2/UVC <85% with $k_1 = 0.0114$ min^{-1} for EF < 97% with $k_1 = 0.0164$ min^{-1} for PEF. TOC removal: 33% for EF < 42% for PEF	Kronka et al. (2020)

(*continued on next page*)

Table 1 (*continued*)

System (anode, cathode)	Pollutant	Experimental remarks	Best results	Ref.
Fig. 1d (Ti|IrO_2–Ta_2O_5 mesh, graphite felt, no oxygen supply)	Ciprofloxacin	2 L of 10–30 mg L^{-1} TOC of drug in pure water, 0.05 M Na_2SO_4, 0.1–0.5 mM Fe^{2+}, pH = 3.0, 25 °C, j = 5–15 mA cm^{-2}, liquid flow rate = 0.4–1.0 L min^{-1}, 15 W UVA light, 420 min	In pure water, total removal in 60 min with k_1 = 0.076 min^{-1} and 77% TOC decay in 420 min for 0.1 mM Fe^{2+}, j = 5 mA cm^{-2}, and liquid flow rate = 0.4 L min^{-1}. Evolution of generated oxalic and oxamic acids by HPLC and released F^-, NO_3^-, and NH_4^+	Cornejo et al. (2023b)
Stirred tank reactor (BDD or Ti/$Ru_{0.5}Ir_{0.5}O_2$ (MMO), carbon felt, injected air)	Penicillin G	150 mL of 50 mg L^{-1} drug in urine, 0.5 mM Fe^{2+}, pH = 3.0, 25 °C, j = 120 mA cm^{-2}, 9 W UVC light, 120 min	TOC decay: 51% for EF-BDD <54% for EF-MMO <65% for PEF-BDD <68% for PEF-MMO. 98%–100% degradation in all cases. Evolution of urea, uric acid, and creatinine	Gonzaga et al. (2021)
Like Fig. 1c (BDD, AISI-304 stainless steel, H_2O_2 addition)	Cephalexin	1 L of 180 mg L^{-1} drug in pure water, 0.1 M Na_2SO_4, 1 mM Fe^{2+}, 50 mg L^{-1} H_2O_2 each 60 min, pH = 3.0, room temperature, j = 10 mA cm^{-2}, liquid flow rate = 7 L min^{-1}, 9 W UVA light, 480 min	Complete removal in 15 min for EF-Fered and PEF-Fered. For the latter, 94% TOC removal, 60% MCE, and EC_{TOC} = 0.10 kWh (g TOC)$^{-1}$. Detection of 6 aromatic by-products and generated fumaric, oxalic, and oxamic acids by HPLC	Antonin et al. (2019)
Real wastewaters rowhead				
Stirred tank reactor upon external light (Fe electrodes, H_2O_2 addition)	Pharmaceutical wastewater	400 mL of wastewater (750 mg L^{-1} COD_0), 0.5–5.0H_2O_2/Fe^{2+}, 0.3–2.5 mL L^{-1} H_2O_2/wastewater, pH = 2.0–5.0, 25 °C, j = 20–80 mA cm^{-2}, 6 W UVA light, 70 min	Optimization by response surface methodology: For EF, 86.85% of COD removal for 3.78H_2O_2/Fe^{2+}, 1.37 mL L^{-1} H_2O_2/wastewater, pH = 2.96, and j = 42.90 mA cm^{-2} for 58.49 min, For PEF, 93.00% of COD removal for 4.29H_2O_2/Fe^{2+}, 1.67 mL L^{-1} H_2O_2/wastewater, pH = 2.91, and j = 43.71 mA cm^{-2} for 54.24 min.	Behfar and Davarnejad (2019)
Like Fig. 1c (BDD, carbon-PTFE air-diffusion)	Landfill leachate	1 L of wastewater (2685 mg L^{-1} COD_0, 1220 mg L^{-1} TOC_0), 7.9 mg L^{-1} total Fe, pH = 3.0, 25 °C, j = 30–90 mA cm^{-2}, liquid flow rate = 200 L h^{-1}, 6 W UVA or UVC light, 240 min	Higher COD and TOC removals with raising j. At 90 mA cm^{-2}, COD removal: 60% (UVA) and 82% (UVC), TOC removal: 70% (UVA) and 92% (UVC). Detection of generated acetic and formic acids by ion chromatography	Crispim et al. (2022)
Homogeneous PEF-like rowhead				
Like Fig. 1a (BDD, Ti/RuO_2, or Ti/IrO_2, carbon-PTFE air-diffusion)	Triclopyr	150 mL of 0.12 mM herbicide in pure water, 0.050 M Na_2SO_4, 0.03–0.09 mM Fe(III)-EDDS [c], pH = 7.0, 35 °C, j = 16.7–66.7 mA cm^{-2}, 6 W UVA light, 300 min	With a BDD anode, 0.06 mM Fe(III)-EDDS, and 25 mA cm^{-2}, complete removal in 90 min and 65% TOC decay in 300 min. Worse performance with the other anodes. 3 heterocyclic, 5 aliphatic, and 2 carboxylic acids by-products identified by GC/MS	Da Costa Soares et al. (2021)
Like Fig. 3a (Ti/Ir–Sn–Ru oxide, stainless steel, with annular photoreactor)	Sulfamethoxazole	3 L of 0.208 mM drug in pure water, 0.025–0.045 M Na_2SO_4 + 0.015–0.035 M NaCl, 0.3–1 mM Fe^{2+}, pH = 3.0, 30 °C, j = 5–20 mA cm^{-2}, liquid flow rate = 180 L h^{-1}, 160 W UVA light, 150 min	Total degradation in 20 min for 0.025 M Na_2SO_4 + 0.015-M NaCl with 0.4 mM Fe^{2+} at j = 15 mA cm^{-2}, 41% TOC reduction in 150 min with EC_{TOC} = 1.136 kWh (g TOC)$^{-1}$.6 aromatic, 6-chloroaromatic, 2-heterocycles, and 2 aliphatic by-products detected by GC/MS	Murrieta et al. (2020a)
Homogeneous SPEF rowhead				
Fig. 1e (Ti/$Ru_{0.3}Ti_{0.7}O_2$, carbon-PTFE air-diffusion)	7 drugs in WWTP effluent	20 L of WWTP, 0.050 M Na_2SO_4, 0.05 mM Fe^{2+}, pH = 3.0, room temperature, j = 20 mA cm^{-2}, liquid flow rate = 570 L h^{-1}, sunlight, 300 min	TOC removal: 19% for AO-H_2O_2 < 25% for EF < 55% for SPEF	Campos et al. (2023)
Like Fig. 1c with a solar CPC [f] photoreactor (BDD, carbon-PTFE air-diffusion)	LAS [g] in greywater	10 L of 40 mg L^{-1} chemical in wastewater, 0.050 M Na_2SO_4, 5 mg L^{-1} Fe^{2+}, pH = 3.0, 25 °C, j = 77.5 mA cm^{-2}, liquid flow rate = 180 L h^{-1}, sunlight, 240 min	Optimization by response surface methodology: 70% removal of LAS and 55% TOC decay of the contaminated greywater	dos Santos et al. (2023)
Fig. S6 (Porous graphite electrodes, air injection)	Petroleum refinery wastewater	1.25 L of wastewater (375 mg L^{-1} COD_0), 0–1 g L^{-1} NaCl, 0.2–0.8 mM Fe^{2+}, pH = 3.0, 30 °C, j = 10–50 mA cm^{-2}, liquid flow rate = 3 L min^{-1}, sunlight, 90 min	Optimization by response surface methodology: 0.747 g L^{-1} NaCl, 0.8 mM Fe^{2+}, j = 10 mA cm^{-2}, and 87 min yielding 93% COD removal with EC_{COD} = 0.01597 kWh (g COD)$^{-1}$	Khaleel et al. (2023)
Homogeneous SPEF-like rowhead				
Like Fig. 1c with a CPC [e] photoreactor (BDD, carbon-PTFE air-diffusion)	Nanofiltration retentate from secondary WWTP effluent	75 L of wastewater (375 mg L^{-1} COD_0), 0.050 M Na_2SO_4, 0.1 mM Fe(III)-EDDS, pH = 3.0, 25–35 °C, j = 74 mA cm^{-2}, liquid flow rate = 300 L h^{-1}, sunlight, 75 min	88% decay of micropollutants with 14.4 kWh m^{-3} energy consumption. Initial addition of 10 mg L^{-1} H_2O_2 reduced 96% of micropollutants with 5.9 kWh m^{-3} energy consumption	Salmeron et al. (2021)
Fig. 3a (Ti/Ir–Sn–Ru oxide, stainless steel with a solar planar photoreactor)	Norfloxacin	3 L of 0.103 mM drug in pure water with 0.015-M NaCl + 0.045 M Na_2SO_4, 0.1–0.5 mM Fe^{2+}, pH = 3.0, 30 °C, j = 5–20 mA cm^{-2}, liquid flow rate = 180 L h^{-1}, 300 min	Overall degradation; 15 min for AO-HClO (k_1 = 0.1999 min^{-1}) < 30 min (k_1 = 0.1278 min^{-1}) for SPEF-HClO with 0.40 mM Fe^{2+} and j = 15 mA cm^{-2}. For the latter process at 300 min, 46% TOC reduction with 2% MCE and EC_{TOC} = 0.76 kWh (g TOC)$^{-1}$	Murrieta et al. (2023)

[a] BDD: Boron-doped diamond.
[b] j: Current density.
[c] MWCNTs: Multiwalled carbon nanotubes.
[d] I: Current.
[e] EDDS: Ethylenediamine-N,N′-disuccinic acid.
[f] CPC: Compound parabolic collector.
[g] LAS: Linear dodecyl-benzene sulfonic acid.

Barazorda-Ccahuana et al. (2023), reporting total mineralization with 40% MCE at the same electrolysis time with a UVC light, as shown in Table 1.

It is remarkable the techno-economic study presented by Mousset et al. (2021) for the mineralization of 1.4 mM phenol (100 mg L^{-1} of initial TOC) in pure water by several AOPs including ozonation, homogeneous Fenton and PF, and homogeneous EF and PEF upon optimized conditions. Ozonation was carried out with a 500 mL glass flask under injection of 300 mg L^{-1} h^{-1} of O_3 at pH = 12.0. Homogeneous Fenton was made in a 600 mL stirred tank reactor with 15.0 mM H_2O_2 and 0.9 mM Fe^{2+} at pH = 3.0, whereas homogeneous PF was carried out in a flow system similar to Fig. 1c with 15.0 mM H_2O_2 and 0.7 mM Fe^{2+} at the same pH using a 263 mL photoreactor exposed to a 12 W UVC light. Homogeneous EF and PEF were performed with the same flow system equipped with a BDD anode and a polyacrylonitrile carbon fiber and adding 0.1 mM Fe^{2+} at j = 12.5 mA cm^{-2}. Fig. S1a shows the expected growth of overall cost for each treatment with raising the mineralization from 50% to 99% because of the much longer time applied. For all the mineralization percentages, the total cost diminished in the sequence: ozonation > homogeneous Fenton > homogeneous PF > homogeneous PEF > homogeneous EF. Note that despite the electric cost of the UVC lamp, homogeneous PF was cheaper than homogeneous Fenton due to the rapid phenol mineralization as a result of the fast photodecomposition of the final Fe(III) carboxylate species from reaction (8). In contrast, the use of the UVC lamp enhanced the total cost of homogeneous PEF for homogeneous EF which also presented a high mineralization rate by the oxidation of such complexes with BDD(•OH) produced by reaction (3). So, the most viable and cost-effective treatment was the homogeneous EF with an overall cost of 125 € m^{-3} (g TOC)$^{-1}$ at 99% mineralization. Figs. S1b–d informs on the percent of sludge, chemicals, and power costs at each mineralization percentage. It can be observed a scarce percent of sludge cost in all cases. A chemical cost >99% was attained for homogeneous Fenton, but for the other methods, the percent of power cost grew concerning that of chemicals costs as the mineralization percentage raised. For the most cost-effective homogeneous EF, 75.8% power cost vs. 24.2% chemicals cost was found at 99% mineralization (see Fig. S1d). Many more studies on the viability and competitiveness of Fenton-based AOPs with different organic pollutants should be performed to show their applicability at the industrial level. Special attention should be made to benchmark the SPEF process where the free sunlight irradiation is expected to offer the best cost-effective process for their mineralization.

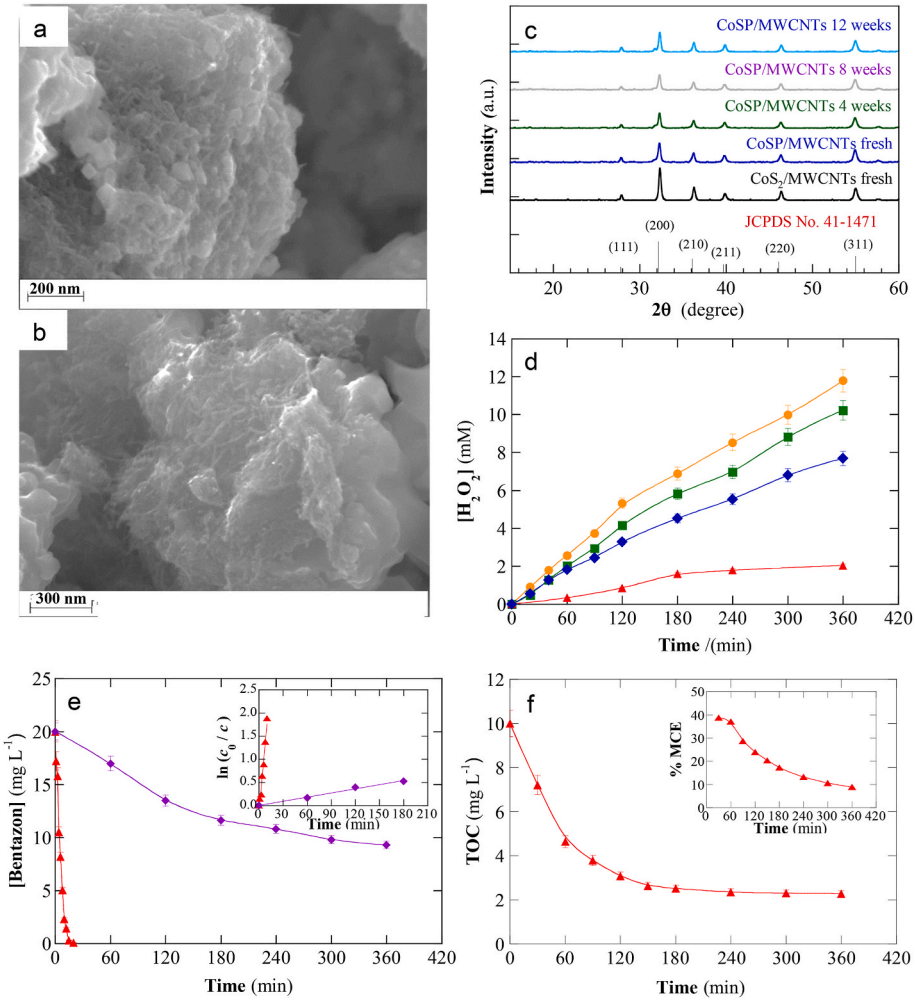

Fig. 2. Field emission scanning electron microscopy (FE-SEM) images of as-synthesized (a) CoS_2/multiwalled carbon nanotubes (MWCNTs) and (b) CoSP/MWCNTs catalysts. (c) X-ray diffraction (XRD) patterns of the above catalysts, compared upon contact with the atmosphere for given periods. Signals related to the pyrite phase of CoS_2 (JCPDS Card No. 41–1471) are given. (d) Change of accumulated H_2O_2 concentration with time for the electrolysis of 2.5 L of a 0.050 M Na_2SO_4 solution at pH 3.0 and 35 °C using a flow plant-like of Fig. 1c with a BDD anode and a (■) CoS2/MWCNTs (●), CoSP/MWCNTs, or (◆) uncatalyzed MWCNTs cathode at j = 25 mA cm^{-2} (▲). Homogeneous PEF treatment of 20 mg L^{-1} bentazon with 0.50 mM Fe^{2+} using a CoSP/MWCNTs cathode and an annular photoreactor with a 160 W UVA lamp. Change of (e) bentazon concentration, with its pseudo-first-order kinetic analysis (inset), and (f) TOC, with its mineralization current efficiency (inset), for the latter assay by (◆) anodic oxidation with electrogenerated H_2O_2 (AO-H_2O_2) and (▲) homogeneous PEF. Adapted from Alcaide et al. (2020).

4.2. Herbicides

Solutions contaminated with herbicides like bentazon (Alcaide et al., 2020), carbaryl (Kronka et al., 2023), clopyralid (Santos et al., 2020), 2, 4-dichlorphenoxyacetic acid (2,4-D) (Forti et al., 2020), diuron + hexazinone (Souza et al., 2019), glyphosate (da Silva et al., 2022), paraquat (Tadayozzi et al., 2021), and tebuthiuron (Da Costa et al., 2021) have been treated by homogeneous PEF.

An interesting article has been published by Alcaide et al. (2020) dealing with the preparation and application of a novel GDE cathode composed of CoSP/multiwalled carbon nanotubes (MWCNTs) deposited onto carbon paper, being compared with a CoS_2/MWCNTs. The field emission scanning electron microscopy (FE-SEM) images of as-synthesized CoS_2/MWCNTs of Fig. 2a and CoSP/MWCNTs of Fig. 2b show that they contained nanocrystals with a cubic-like morphology and a strong enhancement of the CoS_2 and CoSP dispersion without aggregation of particles by the presence of the underlying platform of MWCNTs. Fig. 2c highlights the similar X-ray diffraction (XRD) patterns of both catalysts, which match with the pyrite-phase of CoS_2. It can also be seen that the structure of CoSP/MWCNTs was well stable, remaining its XRD pattern unchanged during 12 weeks in contact with the atmosphere, with an average crystallite size of 27.9 ± 2.0 nm. The concentration of accumulated H_2O_2 with electrolysis time for the treatment of 2.5 L of 0.050 M Na_2SO_4 at pH = 3.0 and 35 °C using a flow plant like Fig. 1c with a BDD anode and different GDE cathodes at $j = 25$ mA cm^{-2} and liquid flow rate = 180 L h^{-1} is depicted in Fig. 2d. As can be seen, more H_2O_2 was accumulated at 350 min in the GDE sequence: CoSP/MWCNTs (11.8 mM) > CoS_2/MWCNTs (10.2 mM) > only carbon paper (7.7 mM). When 20 mg L^{-1} of bentazon was added to the solution with the best GDE with CoSP/MWCNTs and a 160 W UVA light was applied, the corresponding homogeneous PEF process only yielded about 2 mM H_2O_2, as expected by its drastic reduction due to its consumption by Fenton's reaction (5), enhanced from Fe^{2+} regeneration by reactions (6) and (7). This means that homogeneous $^{\bullet}OH$ can be efficiently produced in this system. Under these conditions, Fig. 2e displays the total abatement of the herbicide in 20 min with $k_1 = 0.1875$ min^{-1}, whereas the application of AO-H_2O_2 (without Fe^{2+}) only led to a 53% degradation at 360 min with $k_1 = 0.0030$ min^{-1}, indicating the much smaller oxidation power of BDD($^{\bullet}OH$) formed from reaction (3) than homogeneous $^{\bullet}OH$ from reaction (5). However, Fig. 2f shows that TOC was only reduced by 77% with 12% MCE (see Table 1), suggesting the generation of hardly oxidizable by-products different from carboxylic acids. A study of the decay of toxicity at the end of the process should then be made to know if a biological post-treatment is feasible to remove such recalcitrant by-products and complete the mineralization of the target herbicide. The authors detected the release of SO_4^{2-}, NO_3^-, and NH_4^+ ions, alongside a very low loss of Co from the GDE.

Da Costa et al. (2021) presented a similar homogeneous PEF study by treating 2 L of 100 mg L^{-1} tebuthiuron in pure water with 0.1 M K_2SO_4 and 0.5 mM Fe^{2+} at pH = 3.0 and 25 °C. They also used a flow plant like Fig. 1c with a BDD/carbon-PTFE O_2-diffusion cell by applying a $j = 75$ mA cm^{-2}, liquid flow rate = 50 L h^{-1}, and 64 W m^{-2} UVC light. Despite the use of the more powerful UVC light, a long time of 120 min was required to obtain a 95% removal with $k_1 = 3.2 \times 10^{-4}$ s^{-1}, although with a larger 92% TOC decay in 360 min probably by the predominance of removing carboxylic acids (see Table 1). It was also found a slower degradation by EF with $k_1 = 5.9 \times 10^{-5}$ s^{-1}, being more potent the AO-H_2O_2/UVC process with $k_1 = 2.6 \times 10^{-4}$ s^{-1}, pointing to a synergetic attack of BDD($^{\bullet}OH$) and UVC light over the herbicide. Moreover, the release of NO_3^-, NO_2^-, ClO_2^-, and ClO_3^- ions was detected.

On the other hand, it is noticeable the variant of PEF called PEF-Fered was reported by da Silva et al. (2022) using a stirred tank reactor with Ti/$Ru_{0.3}Ti_{0.7}O_2$ electrodes upon an external 6 W UVC light. Since the cathode did not produce H_2O_2, this compound was directly added to the solution. The trials were performed with 100 mL of 100 mg L^{-1} glyphosate in pure water containing 0.050 M Na_2SO_4, 10 mg L^{-1} Fe^{2+}, and 100 mg L^{-1} H_2O_2 at pH = 3.0, room temperature, and $j = 50$ mA cm^{-2} lasting 120 min. The homogeneous PEF-Fered gave 74% degradation, 86% COD abatement, and 85% TOC removal and the effect of the UVC light was demonstrated by its superiority over the analogous homogeneous EF-Fered that yielded lower values of 70% degradation, 82% COD abatement, and 79% TOC removal (see Table 1).

4.3. Dyes

The application of homogeneous PEF to the remediation of dyeing waters has been carried out for Bismark Brown G, Bismark Brown R, and Brown DGI (Medrano-Rodriguez et al., 2020), Brown HT (Corona-Bautista et al., 2021). Chocolate Brown HT and Eriochrome Black (Pacheco-Alvarez et al., 2019), Direct Red 23 (Titchou et al., 2022), Eosin Yellow (Mansour et al., 2023), Erythrosine B (Clematis and Panizza, 2021), Methyl Orange (Kong et al., 2020; Marquez et al., 2020). Orange G (Liu et al., 2019), Reactive Blue 4 (Nakamura et al., 2019), and Red CL and Red WB (Herrera-Chavez et al., 2024).

Figs. S2a and b show the corresponding decay in color and TOC for the homogeneous EF and PEF treatments of 150 mL of 36.2 mM Reactive Blue 4 dye in pure water containing 0.050 M Na_2SO_4 or 0.15 M NaCl and 0.5 mM Fe^{2+}at pH = 3.0 and 35 °C. The system was a conventional stirred tank reactor similar to Fig. 1a with a Ti/$Ru_{0.15}Ti_{0.85}O_2$ anode and a carbon-PTFE air-diffusion cathode operating at $I = 100$ mA upon 12 W UVA light (Nakamura et al., 2019)). A quite similar discoloration rate of the dye can be observed in Fig. S2a for homogeneous EF and PEF with 0.050 M Na_2SO_4, reaching 94% loss of color in 70 min, as expected by a slow regeneration of Fe^{2+} from reactions (6) and (7). In contrast, the same percentage of color was lost in a shorter time of 30 min for homogeneous PEF with 0.15 M NaCl due to the parallel oxidation with active chlorine (HClO) produced from reactions (12) and (13) that enhanced the loss of color of the dye. The authors demonstrate the positive action of the incident UVA light over TOC removal. Fig. S2b makes evident that after 360 min of electrolysis in 0.050 M Na_2SO_4, 70% mineralization was achieved by homogeneous PEF, much greater than 33% determined by homogeneous EF (see Table 1), as a result of the fast photodecarboxylation of recalcitrant Fe(III)-carboxylate species from reaction (8).

Clematis and Panizza (2021) reported the homogeneous EF, PEF, and SPEF processes of 300 mL of 100 mg L^{-1} Erythrosine B dye in pure water with 0.050 M Na_2SO_4 and 0.1 mM Fe^{2+} at pH = 3.0 and room temperature using a stirred tank reactor like of Fig. 1a with a BDD anode and a carbon felt cathode at $j = 20$ mA cm^{-2} under 50 or 100 W UVA light. Fig. S2c highlights a similar percentage of color removal for homogeneous PEF with 100 W UVA light and SPEF that yielded overall discoloration in 20 min. The homogeneous PEF with 25 W UVA light was less potent due to the incidence of a smaller quantity of photons, giving rise to a colorless solution in a longer time of 35 min. However, it was able to regenerate amount enough of Fe^{2+} from reaction (7) accelerating Fenton's reaction (5) to be more powerful than homogeneous EF that required 50 min for total loss of color. A similar tendency can be seen in Fig. S2d for the percentage of COD removal since total mineralization was attained in 90 min for homogeneous PEF with 100 W UVA light and SPEF, whereas 97% and 91% of COD were abated after 120 min of homogeneous PEF with 25 W UVA light and EF, respectively (see Table 1). These findings demonstrate that homogeneous PEF can possess a similar oxidation power to homogeneous SPEF using a UVA light with high power enough, although with a much higher operating cost by the electricity consumed by the UVA lamp. A similar work by Titchou et al. (2022) considered the effect of NaCl by treating 230 mL of 80 mg L^{-1} Direct Red 23 in pure water with 0.050 M Na_2SO_4 or 0.10 M NaCl and 0.1 mM Fe^{2+} at pH = 3.0, 20 °C, and $j = 2.5$–15 mA cm^{-2}under a UVA LED light ($\lambda = 400$ nm). Table 1 shows that discoloration was enhanced at higher j due to the increasing generation of more oxidizing agents, as pointed out above. Faster loss of color was found for NaCl vs, Na_2SO_4 because of the quicker parallel oxidation of the dye with generated

active chlorine. However, after 360 min at $j = 5$ mA cm^{-2}, a 95% TOC decay was obtained for homogeneous PEF in Na_2SO_4, which was reduced to 76% in NaCl due to the formation of recalcitrant chlorderivatives. This loss of performance is then expected in chloride media such as real wastewater.

It is interesting to note that a 2D BDD cathode can offer an excellent performance for homogeneous PEF as well. Corona-Bautista et al. (2021) treated 160 mL of 50 and 80 mg L^{-1} Brown HT dye in pure water with 0.050 M Na_2SO_4 and 0.5 mM Fe^{2+} at pH = 3.0 and room temperature using a stirred BDD/BDD tank reactor at $j = 71$ mA cm^{-2} and 75 mW cm^{-2} UVA light for 60 min. Total color removal with a similar discoloration rate was found for homogeneous EF and PEF, with $k_{dis} = 0.120$ min^{-1} for 50 mg L^{-1} dye that dropped to $k_{dis} = 0.085$ min^{-1} for higher 80 mg L^{-1} dye (see Table 1). Moreover, an 80% COD abatement was determined for the former conditions at such time for homogeneous PEF. The analysis of the treated solution by ion-exclusion HPLC allowed following the evolution of generated glyoxylic, oxalic, and oxamic acids.

4.4. Drugs

Drugs such as acebutolol (Daniel et al., 2020; Zhang et al., 2022), amitriptyline (Melin et al., 2021), ampicillin (Cornejo et al., 2023c), carbenicillin (Ren et al., 2023), cephalexin (Antonin et al., 2019), ciprofloxacin (Cornejo et al., 2023b), paracetamol (Pinheiro et al., 2019; Kronka et al., 2020), penicillin G (Gonzaga et al., 2021), sulfamethazine (Wang et al., 2020), and sulfamethoxazole and trimethoprim (Delgado-Vargas et al., 2022), have been treated in aqueous solutions with homogeneous PEF.

Several authors have used simple stirred tank reactors similar to Fig. 1a with unmodified or modified GDE cathodes. So, Zhang et al. (2022) detailed the treatment of 150 mL of 0.046 mM acebutolol (10 mg L^{-1} TOC_0) in pure water containing 0.05 M Na_2SO_4 and 0.5 mM Fe^{2+} at pH = 3.0 and 25 °C. The cell was equipped with a Ti/RuO_2 anode and an agarose-derived carbon-PTFE air-diffusion at $j = 60$ mA cm^{-2} and submitted to a 6 W UVA light. A very fast and complete drug removal in 9 min with $k_1 = 0.477$ min^{-1} was found and an excellent 90% TOC abatement was obtained in 360 min (see Table 1). The good oxidation power of the system was compared with that of a WWTP matrix of 10.4 mg L^{-1} TOC. The presence of organic matter and inorganic anions consuming the oxidizing agents slowed down the process in the WWTP, reaching total degradation in 60 min and being TOC removed by 47% in 360 min. Another study by Ren et al. (2023) was centered over 150 mL of 0.049 mM carbenicillin in simulated and WWTP effluents by adding 0.010 M Na_2SO_4 and 0.50 mM Fe^{2+} at pH = 3.0 and 25 °C using a BDD/carbon-PTFE air-diffusion cell at $I = 20$ mA under 6 W UVA light. Using only the pure sulfate solution, 13 min were required for overall abatement, which was raised to 15 min for simulated and 18 min for WWTP (see Table 1). After 480 min of electrolysis, TOC was reduced by 95% in pure sulfate solution, decreasing to an acceptable 80% in WWTP, pointing to a good oxidation power of the system under real conditions. HPLC analysis of the treated sulfate solution revealed the generation of 23 aromatic by-products, 7 aliphatic derivatives, and 7 final carboxylic acids. On the other hand, the treatment of 450 mL of 180 mg L^{-1} paracetamol in pure water with 0.1 M K_2SO_4 and 0.15 mM Fe^{2+} at pH = 2.0 and 20 °C filling a BDD/modified carbon-PTFE O_2-diffusion with 1, 4-naphthoquinone cell at $j = 75$ mA cm^{-2} under UVC light lasting180 min has been reported by Kronka et al. (2020). At such time, 97% drug decay with $k_1 = 0.0164$ min^{-1} and 42% TOC removal for homogeneous PEF was found, upgrading an 85% decay with $k_1 = 0.0114$ min^{-1} and 33% TOC removal found for homogeneous EF (see Table 1). These findings confirm the acceleration of $^{\bullet}$OH generation by Fenton's rection (5) from Fe^{2+} regeneration by reaction (7) and pre-eminently, H_2O_2 photolysis by reaction (9), alongside the photodecomposition of Fe(III) species by reaction (8). The authors corroborated the high $^{\bullet}$OH production by measuring a 74–76% degradation with $k_1 = 0.0082$ min^{-1} for AO-H_2O_2 and AO-H_2O_2/UVC, indicating that the drug was largely removed by reactive BDD($^{\bullet}$OH) with little participation of its photolysis by UVC light.

A curious work of Cornejo et al. (2023b) described the ciprofloxacin removal in pure water using the flow system of Fig. 1e equipped with the flow-through filter-press cell of Fig. 1d with a Ti|IrO_2–Ta_2O_5 mesh anode and a graphite felt cathode. No O_2 was supplied because that produced at the anode was assumed to be sufficient for the electrogeneration of H_2O_2 from reaction (1). The assays were carried out with 2 L of 10–30 mg L^{-1} TOC of the drug by adding 0.05 M Na_2SO_4 and 0.1–0.5 mM Fe^{2+} at pH = 3.0, 25 °C, $j = 5$–15 mA cm^{-2}, and liquid flow rate = 0.4–1.0 L min^{-1} upon 15 W UVA light lasting 420 min. A total abatement was found in 60 min with $k_1 = 0.076$ min^{-1} and 77% of final TOC decay for 0.1 mM Fe^{2+}, $j = 5$ mA cm^{-2}, and liquid flow rate = 0.4 L min^{-1}. It detected the formation of oxalic and oxamic acids as final by-products by HPLC, alongside the release of F^-, NO_3^-, and NH_4^+ ions from the F and N atoms present in the drug.

Urine is a complex matrix that contains urea, uric acid, and creatinine as main organic components, which can be oxidized by $^{\bullet}$OH and active chlorine. Gonzaga et al. (2021) studied the mineralization of Penicillin G in urine with a stirred tank reactor with a BDD or Ti/$Ru_{0.5}Ir_{0.5}O_2$ (metal mixed oxide, MMO) anode and a carbon felt cathode. A volume of 150 mL of this medium with 50 mg L^{-1} drug and 0.5 mM Fe^{2+} at pH = 3.0, 25 °C, and $j = 120$ mA cm^{-2} was submitted to 9 W UVC light during 120 min. Almost total degradation was achieved for homogeneous EF and PEF with both anodes. In contrast, a partial TOC removal was attained depending on the process: 51% for EF with BDD <54% for EF with MMO <65% for PEF with BDD <68% for PEF with MMO (see Table 1). The MMO anode was more powerful than the BDD one, suggesting a superior reactivity of the greater amount of active chlorine formed at the former anode with all the organics of the urine matrix. This means that the nature of the aqueous matrix can largely affect the oxidation ability of the homogeneous PEF, and cheaper DSA anodes can be even more potent than BDD ones.

Antonin et al. (2019) studied the homogeneous PEF-Fered process of cephalexin with a flow system like Fig. 1c with a BDD anode and an AISI-304 stainless steel cathode filled with 1 L of 180 mg L^{-1} drug in pure water with 0.1 M Na_2SO_4 and 1 mM Fe^{2+} at pH = 3.0 and room temperature. To do the trials, 50 mg L^{-1} of H_2O_2 was added each 60 min and a $j = 10$ mA cm^{-2}, and liquid flow rate = 7 L min^{-1} were applied under illumination with a 9 W UVA light lasting 480 min. Fig. S3a shows an enhancement of the overall cephalexin content removal in the order: AO (4 h) > AO/UVA (3 h) > homogeneous EF-Fered = homogeneous PEF-Fered (15 min). This indicates again the much superior oxidation power of $^{\bullet}$OH produced from Fenton's reaction (5) than BDD($^{\bullet}$OH) generated from reaction (3). When TOC was determined, Fig. S3b reveals that its final removal of 97% was much greater, as expected, for homogeneous PEF-Fered (see Table 1). This process also presented the higher values of the percentage of MCE (see Fig. S3c), which dropped with time up to 60%. This decay is related to 2 effects: the gradual loss of organic load and the accumulation of more recalcitrant intermediates. The opposite trend can be observed in Fig. S3d for the EC_{TOC} profile that raised with time up to a low value of 0.10 kWh (g TOC)$^{-1}$, without considering the cost of the UVA lamp. 6 aromatic by-products and generated fumaric, oxalic, and oxamic acids were detected by HPLC. The evolution of oxalic and oxamic acids is presented in Figs. S3e and S3f, respectively. Oxalic acid was more largely accumulated in homogeneous EF-Fered, dramatically decaying in homogeneous PEF-Fered as a result of the photolysis of Fe(III)-oxalate complexes, which can explain the higher TOC removal of the latter method. In contrast, a slightly smaller amount of oxamic acid was found for the latter process with respect to the former one, indicating a smaller photolysis of Fe(III)-oxamate species.

4.5. Real wastewaters

Excellent homogeneous PEF treatment of real wastewater has been

reported. Pharmaceutical wastewater (Behfar and Davarnejad, 2019), sulfidic spent caustic (Esfahani et al., 2019), dairy wastewater (Bruguera-Casamada et al., 2019), landfill leachate (Crispim et al., 2022), and distilling industry wastewater (Perumal et al., 2023) have been examined. Echeverry-Gallego et al. (2023) demonstrated that this procedure reduced the abundance of genes related to pathogenicity factors, antibiotic resistance, and metabolism.

For pharmaceutical wastewater with 750 mg L^{-1} COD_0, Behfar and Davarnejad (2019) proposed a photo-assisted electrocoagulation with H_2O_2 addition as a variant of homogeneous PEF. The stirred tank reactor contained two Fe electrodes, so that, the Fe anode was oxidized and solubilized to Fe^{2+} as follows:

$$Fe \rightarrow Fe^{2+} + 2e^- \quad (20)$$

Despite this reaction, additional Fe^{2+} was added to the medium to enhance the H_2O_2 decomposition by Fenton's reaction (5). Response surface methodology was utilized to optimize the assays made with 400 mL of wastewater, 0.5–5.0H_2O_2/Fe^{2+} molar ratio, and 0.3–2.5 mL L^{-1} H_2O_2/wastewater at pH = 2.0–5.0, 25 °C, and j = 20–80 mA cm^{-2} submitted to 6 W UVA light during 70 min. Good optimum results were found for homogeneous EF, which were upgraded for homogeneous PEF, as can be seen in Table 1.

It is interesting to the recent article published by Crispim et al. (2022) who studied the influence of j and the kind of UV light on the remediation of landfill leachate with 2685 mg L^{-1} COD_0 and 1220 mg L^{-1} TOC_0. They used a flow system like Fig. 1c with a BDD/carbon-PTFE air-diffusion cell for treating 1 L of wastewater with 7.9 mg L^{-1} total Fe at pH = 3.0, 25 °C, j = 30–90 mA cm^{-2}, and liquid flow rate = 200 L h^{-1} under 6 W of UVA or UVC light during 240 min. Figs. S4a and S4b show an enhancement of both, COD and TOC abatements with raising j and using UVC light, respectively. The increase at higher j can be ascribed to the concomitant production of more oxidizing agents and the superiority of UVC light to the additional generation of $^{\bullet}OH$ from electrogenerated H_2O_2 via reaction (9). For the greater j = 90 mA cm^{-2}, COD removal of 60% with UVA and 82% for UVC was obtained, whereas TOC was reduced by 70% with UVA and 92% with UVC (see Table 1). Fig. S4c highlights the enhancement of the energy consumption per g of TOC considering the energy provided by each UV lamp with j due to the high rise of E_{cell}. This energetic parameter is always slightly smaller with UVC due to its higher oxidation power. However, less energy consumption was found up to j = 60 mA cm^{-2} for homogeneous EF with much lower oxidation power, being quite similar to both homogeneous PEF processes at j = 90 mA cm^{-2}. These findings agree with the results reported above in Fig. S1 by Mousset et al. (2021) in which the homogeneous EF is more cost-effective due to the high energy cost of the UV lamp.

5. Homogeneous photoelectro-Fenton-like

A homogeneous PEF-like process operating at neutral pH has been proposed by stabilizing Fe^{2+} upon the addition of the quencher EDDS (ethylenediamine-N,N′-disuccinic acid) (Ye et al., 2020a; Da Costa Soares et al., 2021). These authors presupposed that the target molecule can be oxidized by M($^{\bullet}OH$) generated from reaction (3) and HClO from reactions (12) and (13), Moreover the Fe(III)-EDDS complex reacted with electrogenerated H_2O_2 to form the Fe(II)-EDDS one by reaction (21), which yields homogeneous $^{\bullet}OH$ from the Fenton-like reaction (22). Additionally, the complex can be photo-reduced by reaction (23) to originate Fe^{2+} that can yield $^{\bullet}OH$ from Fenton's reaction (5).

$$Fe(III)\text{-}EDDS + H_2O_2 \rightarrow Fe(II)\text{-}EDDS + O_2^{\bullet-} + 2H^+ \quad (21)$$

$$Fe(II)\text{-}EDDS + H_2O_2 \rightarrow Fe(III)\text{-}EDDS + {}^{\bullet}OH + OH^- \quad (22)$$

$$Fe(III)\text{-}EDDS + h\nu \rightarrow Fe^{2+} + EDDS^{\bullet+} \quad (23)$$

Fig. S5a depicts the effect of the anode over the time course of accumulated H_2O_2 content for 50 mL of 0.12 mM triclopyr (10.0 mg L^{-1} TOC_0) with 0.025 M Na_2SO_4 + 0.035 M NaCl and 0.06 mM (7.2 mg L^{-1} TOC_0) Fe(III)–EDDS (1:1) at pH 7.0 and 35 °C using a system like of Fig. 1c at j = 25 mA cm^{-2} uòn a 6 W UVA light (Da Costa Soares et al., 2021). As can be seen, H_2O_2 accumulation decreased in the sequence: BDD > RuO_2-based anode > IrO_2-based anode. The decay of H_2O_2 can be mainly ascribed to its oxidation at the surface of anode M to O_2 via the intermediate reaction (2) originating the weak oxidant $HO_2^{\bullet}$, a reaction that was then slower for BDD.

Fig. S5b reveals that active chlorine was more favorably produced in the order: of RuO_2-based anode > IrO_2-based anode > BDD anode. The fact that BDD accumulated more H_2O_2 explained the slightly quicker and total removal of the Fe(III)-EDDS complex attained in 90 min, as can be seen in Fig. S5c. The corresponding k_1-values were 0.0982 min^{-1} for BDD >0.0888 min^{-1} for RuO_2-based >0.0793 min^{-1} for IrO_2-based. Fig. S5d highlights that the herbicide triclopyr was also more rapidly abated with BDD suggesting its quicker removal with homogeneous $^{\bullet}OH$ than active chlorine. Its k_1-value decreased as 0.0251 min^{-1} for BDD >0.0221 min^{-1} for RuO_2-based >0.0168 min^{-1} for IrO_2-based. The same tendency was found for TOC reduction (see Fig. S5e), with 65% mineralization attained in 300 min using BDD (see Table 1). The excellent results obtained for BDD, slightly worse for the other two DSA anodes, validate the application of this procedure at pH = 7.0. However, its main drawback is the introduction of another organic like EDDS that increases the organic load due to the herbicide solution and the difficulty of its mineralization.

Another homogeneous PEF-HClO treatment has been proposed by Murrieta et al. (2020a) considering the photo-assisted electrochemical generation of HClO from reactions (12) and (13) and the production of Fe^{2+} from reactions (6) and (7) as Fenton-like reagents in chloride media. HClO can then directly oxidize the organics or react with Fe^{2+} to yield homogeneous $^{\bullet}OH$ as follows:

$$HClO + Fe^{2+} \rightarrow Fe^{3+} + Cl^- + 2{}^{\bullet}OH \quad (24)$$

The flow system used was the same as Fig. 3a but with an annular photoreactor containing a 160 W UVA light, in which 3 L of 0.208 mM sulfamethoxazole in pure water with 0.025 M Na_2SO_4 + 0.015-M NaCl and 0.4 mM Fe^{2+} at pH = 3.0, 30 °C, and j = 15 mA cm^{-2} were rapidly and completely degraded in 20 min (see Table 1). After 150 min of electrolysis, TOC was abated by 41% with an EC_{TOC} = 1.136 kWh (g TOC)$^{-1}$. Parallel GC/MS analysis of the treated solution allowed the identification of 6 aromatic, 6-chloroaromatic, 2-heterocycles, and 2 aliphatic by-products.

6. Homogeneous solar photoelectro-Fenton

PEF with sunlight irradiation or SPEF has been developed to obtain a more useful process in practice because it is more efficient and cost-effective than PEF with artificial lamps. Homogeneous SPEF has been checked for the remediation of Orange II dye (Paz et al., 2020) and 3 antibiotics and 2 non-steroidal anti-inflammatories in pure wáter (Bugueno-Carrasco et al., 2021), 7 drugs in WWTP effluent (Campos et al., 2023), and linear dodecyl-benzene sulfonic acid. (LAS) in grey-water (dos Santos et al., 2023), along with different recalcitrant wastewaters like industrial textile wastewater (Salazar et al., 2019), elderberry agro-industrial water (Ferreira et al., 2020), UWWTP effluents (Deemter et al., 2022), industrial wastewater (Salazar et al., 2022), and petroleum refinery wastewater (Khaleel et al., 2023).

The work of Campos et al. (2023) was centered on clarifying the performance of a flow raceway pond reactor upon sunlight connected to a single filter-press cell, as schematized in Fig. 1e. The cell contained a DSA anode of $Ti/Ru_{0.3}Ti_{0.7}O_2$ and a carbon-PTFE air-diffusion cathode with recirculation of 20 L of a WWTP effluent contaminated with 100 μg L^{-1} of progesterone, estradiol, ibuprofen, diclofenac, estrone, sulfamethazine, and carbamazepine. Contents of 0.050 M Na_2SO_4, and 0.05 mM Fe^{2+} were added to such contaminated WWTP at pH = 3.0 and room

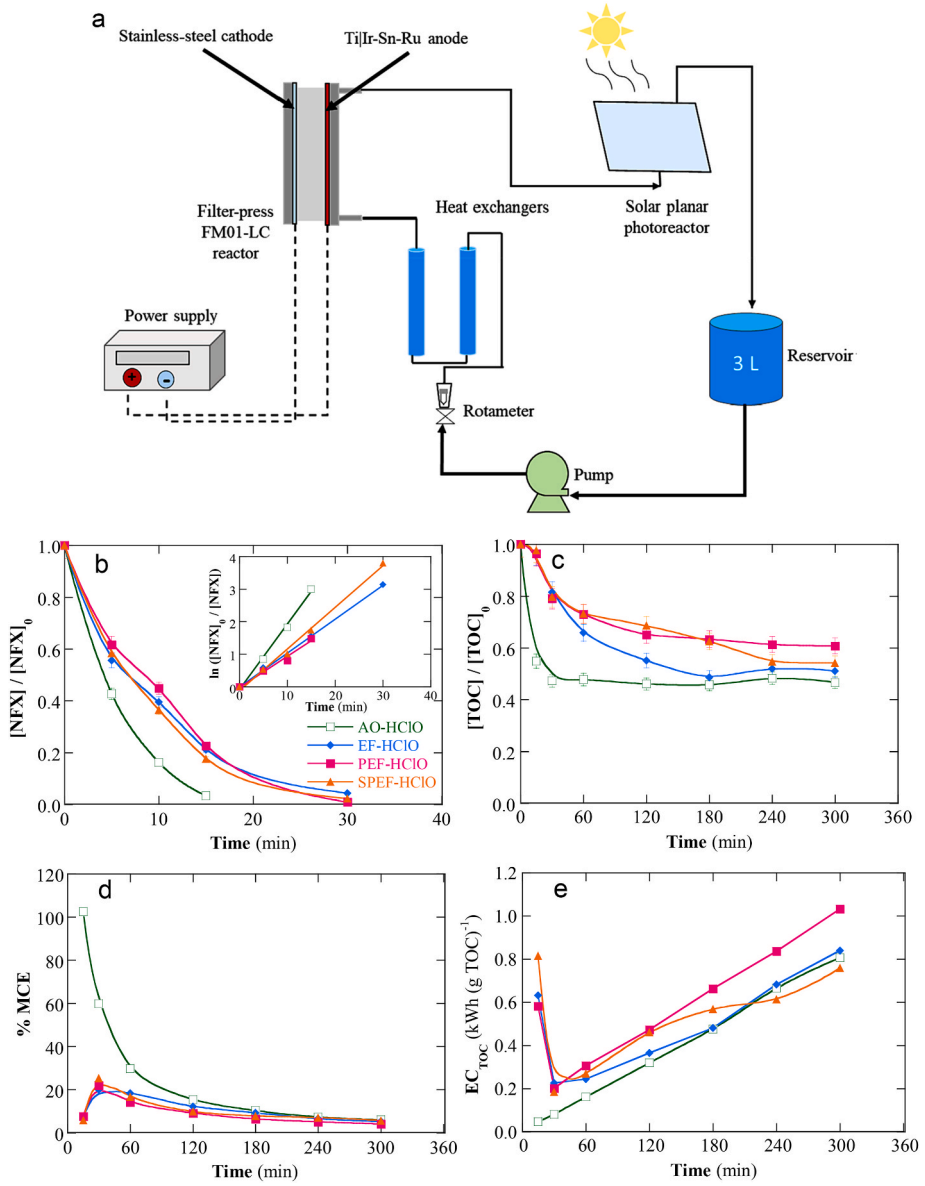

Fig. 3. (a) Sketch of the experimental setup of the solar flow plant used for the homogeneous SPÊF-like process with a Ti/Ir–Sn–Ru anode, a stainless-steel cathode, and a solar planar photoreactor of norfloxacin (NFX) in chloride medium. Time course of (b) normalized NFX content and kinetic analysis (inset), (c) normalized TOC, (d) mineralization current efficiency, and (e) energy consumption per g of TOC for 3 L of 0.103 mM (20 mg L^{-1} TOC_0) drug in pure water with 15 mM NaCl + 45 mM Na_2SO_4 at pH 3.0 and 30 °C by AO-HClO, EF-HClO, PEF-HClO, and SPEF-HClO at j = 15 mA cm^{-2} and liquid flow rate = 180 L h^{-1}. For the Fenton-based processes, 0.40 mM Fe^{2+} was added as a catalyst, and in the homogeneous PEF-HClO, an annular photoreactor of 600 mL with an internal 160 W UVA lamp was used. Adapted from Murrieta et al. (2023).

temperature, and a j = 20 mA cm^{-2} and liquid flow rate = 570 L h^{-1} were applied for 300 min. It was found an increase in the final TOC abatement of 19% for AO-H_2O_2 < 25% for homogeneous EF < 55% for homogeneous SPEF. All the drugs were largely removed in the latter process and its high efficiency was ascribed to the large contact area between the effluent and UV irradiation of sunlight in the flow raceway pond reactor.

Another article by dos Santos et al. (2023) degraded LAS in grey-water using a flow system like Fig. 1c with a BDD/carbon-PTFE air--diffusion filter-press and a solar compound parabolic collector (CPC) photoreactor. The optimization of the homogeneous SÊF treatment of 10 L of 40 mg L^{-1} of this chemical in the wastewater was found for 0.050 M Na_2SO_4, 5 mg L^{-1} Fe^{2+}, pH = 3.0, 25 °C, j = 77.5 mA cm^{-2}, liquid flow rate = 180 L h^{-1}, and 240 min. Under these conditions, LAS was removed by 70% and TOC was reduced by 55% (see Table 1), which are excellent results because of the high recalcitrance of the chemical and wastewater checked.

To study the remediation of a petroleum refinery wastewater with 375 mg L^{-1} COD_0 by homogeneous SPEF, Khaleel et al. (2023) used the flow system with a solar CPC photoreactor of Fig. S6a equipped with the flow-by graphite/graphite filter-press cell of Fig. S6b. The tests were made with 1.25 L of wastewater by addition of 0–1 g L^{-1} NaCl and 0.2–0.8 mM Fe^{2+} at pH = 3.0, 30 °C, j = 10–50 mA cm^{-2}, and liquid flow rate = 3 L min^{-1} lasting 90 min. The process was optimized by response surface methodology and the best variables were 0.747 g L^{-1} NaCl, 0.8 mM Fe^{2+}, j = 10 mA cm^{-2}, and 87 min (see Table 1). For these conditions, am excellent 93% COD removal with EC_{COD} = 0.01597 kWh (g COD)$^{-1}$ was determined, pointing to a good viability of this procedure for the treatment of petroleum refinery wastewater at an industrial scale.

7. Homogeneous solar photoelectro-Fenton-like

Like homogeneous PEF-like, the works of homogeneous SPEF-like were centered on the addition of the quencher EDDS (Salmeron et al., 2021) and the application of a novel process with simultaneous HClO and Fe^{2+} electrogeneration (Murrieta et al., 2020b, 2023). Salmeron et al. (2021) treated a secondary WWTP effluent after concentration as nanofiltration retentate with 375 mg L^{-1} COD_0 through a flow plant-like of Fig. 1c with a BDD/carbon-PTFE air-diffusion filter-press cell coupled to a solar CPC photoreactor. A volume of 75 L of the wastewater with 0.050 M Na_2SO_4 and 0.1 mM Fe(III)-EDDS (1:1) at pH = 3.0 and 25–35° was treated at $j = 74$ mA cm^{-2} and liquid flow rate = 300 L h^{-1} lasting 75 min. Micropollutants measured by HPLC in the wastewater dropped 88% on average with EC = 14.4 kWh m^{-3}. Since the procedure electrogenerated a small amount of H_2O_2, its oxidation power was upgraded by initially adding 10 mg L^{-1} of this compound, and fit was found that the degradation of micropollutants grew up to 96% with only EC = 5.9 kWh m^{-3} (see Table 1), showing its viability at industrial level.

Fig. 3a schematizes the solar flow plant used for the homogeneous SPEF-HClO process of norfloxacin (NFX) in a chloride medium (Murrieta et al., 2023). The filter-press cell contained a Ti/Ir–Sn–Ru anode and a stainless-steel cathode connected to a solar planar photoreactor. First, the tests were performed by recirculating 3 L of 0.103 mM drug in pure water with 0.015-M NaCl +0.045 M Na_2SO_4 and 0.4 mM Fe^{2+} at pH = 3.0, 30 °C, $j = 15$ mA cm^{-2} and liquid flow rate = 180 L h^{-1} for 300 min. Fig. 3b–e shows the time course of normalized NFX content and TOC, percentage of MCE, and EC_{TOC} for different processes. Surprisingly, better performance was found for homogeneous AO-HClO (without Fe^{2+}) than Fenton-based EAOPs. So, the drug disappeared from the medium in only 15 min with $k_1 = 0.1999$ min^{-1} for the former process, whereas a longer time of 30 min for homogeneous EF-HClO, PEF-HClO, and SPEF-HClO with $k_1 = 0.1278$ min^{-1} (see Table 1). Nevertheless, for the homogeneous SPEF-HClO at 300 min, a 46% TOC reduction with 2% MCE and EC_{TOC} = 0.76 kWh (g TOC)$^{-1}$ was found, with values quite similar to those of homogeneous AO-HClO. The lower performance of homogeneous SPEF-HClO was ascribed to a drastic loss of its oxidation ability by the conversion of the stronger oxidant HClO into the weaker one $^{\bullet}OH$ from the reaction (24). This was confirmed by the decay of normalized drug content with increasing the addition of Fe^{2+} from 0.1 to 0.5 mM, as can be seen in Fig. S7a. In contrast, Fig. S7b shows a much poorer TOC reduction with 0.1 mM Fe^{2+}, suggesting a faster destruction of chloroderivatives formed when more quantity of $^{\bullet}OH$ is produced at higher Fe^{2+} content. The authors also confirmed the oxidation power of the homogeneous SPEF-HClO power under comparative conditions with a WWTP effluent. The consumption of oxidants with its organic components and inorganic ions inhibited the removal of NFX. Fig. S7c highlights that in WWTP effluent, 30 min were also needed for overall degradation with a smaller $k_1 = 0.0784$ min^{-1}, whereas Fig. S7d reveals a lower TOC reduction up to 40%. These findings point to consider that this treatment only possesses a slightly lower oxidation power in real wastewater than in pure water. Moreover, the by-products that originated in pure water were identified by LC-MS/MS and the initial degradation sequence of NFX (**1**) shown in Fig. S7e was proposed. The initial attack of $^{\bullet}OH$ on the C(3) of the piperazine group of **1** gives the hydroxylated compound **2** that is transformed into **5** with breaking of the piperazine group or **6** with a carbonyl addition on its C(2). Further oxidation of **5** and **6** originates **7** with two carbonyls linked to the two N atoms of the broken piperazine group that further yields **8** losing the carbonyl joined to the N atom linked to the naphthalene ring. The parallel chlorination over C(9) of the naphthalene ring of **1** forms **3**, followed by the loss of the piperazine group to give **9**. The hydroxylation in C(7) of the naphthalene group of **1** with the release of F^- yields **4**, whose naphthalene ring is broken to form **10**, followed by its hydroxylation and decarboxylation leading to **11**.

8. Heterogeneous photoelectro-Fenton

Few heterogeneous PEF processes have been proposed aiming to operate at neutral pH with low production of iron hydroxide sludge. A first approach considered solid iron catalysts to remove the chemical 1-butyl-2,3-dimethylimidazolium with a Fe/TiO_2/perlite catalyst (Diez et al., 2020), the dyes Sunset Yellow with Fe_3O_4 (Pinheiro et al., 2020) and Ponceau SS with vermiculite (dos Santos et al., 2020), and the drugs thiamphenicol with pyrite (Thiam et al., 2020), carbamazepine with NOM (Duan and Sedlak, 2024), cephalexin with chalcopyrite (Droguett et al., 2020), and tetracycline with Fe/C/N/ZIF-8/ACF (Zhang et al., 2024). A second approach was based on functionalized GDE cathodes applied for the treatment of bisphenol S with Co-porphyrin/Printex L6 GDE (Marques et al., 2022), the dyes Methyl Orange, Methylene Blue, and Rhodamine B with bismuth hexacyanoferrate/graphene/carbon fibers GDE (Chen et al., 2022), and the dye Methylene Blue and the drug erythromycin with graphene-MOFs (2Fe/Co)/CNF cathode membrane (Li et al., 2023a). Table 2 lists selected results of these works, On the other hand, a sensor for H_2O_2 detection using heterogeneous PEF with iron sites on graphdiyne has been detailed by Li et al. (2023b).

Fig. S8a shows a sketch of the setup of the heterogeneous PEF treatment of 1-butyl-2,3-dimethylimidazolium in aqueous medium (Diez et al., 2020). It consisted of an electrochemical cell with a BDD anode and a carbon felt cathode upon air injection linked to a photocell containing a floating Fe/TiO_2/perlite catalyst under illumination with a 250 nm UVA-LED lamp. A volume of 320 mL of 25 mg L^{-1} chemical in pure water or WWTP with 0.010 M Na_2SO_4 at natural pH and 20 °C was recirculated through this system for 240 min. An $I = 50$ mA was applied to the electrochemical cell and 2.72 g L^{-1} catalyst was added to the photocell. Fig. S8b depicts that the faster chemical abatement was reached with the Fe/TiO_2/perlite catalyst with total disappearance in 120 min. A slightly slow abatement can be observed for Fe/perlite catalyst giving rise to total removal at the same time. When TiO_2/perlite was used as a catalyst, the chemical was more slowly removed up to 98% at 120 min. For these catalysts, it is expected the production of heterogeneous $^{\bullet}OH$ from reaction (10) from the surface $\equiv Fe^{2+}$ onto Fe and perlite (an aluminum potassium sodium silicate mineral with <1% Fe_2O_3) with electrogenerated H_2O_2. $\equiv Fe^{2+}$ can thus be regenerated from the formed $\equiv Fe^{3+}$ by a surface photolytic reaction similar to (7). Moreover, TiO_2 is a common photocatalyst that originates oxidizing agents like $^{\bullet}OH$, as explained in subsection 9a, but this point was disregarded by the authors. The synergy action of the three components of Fe/TiO_2/perlite then possessed more oxidation power than simpler combinations due to the greater heterogeneous $^{\bullet}OH$ generation, including that of BDD($^{\bullet}OH$) formed at the anode from reaction (3). Fig. S8c highlights a large ability of the heterogeneous PEF to abate the COD in 80% and TOC in 70% of the solution in pure water at 240 min (see Table 2). These good results can be associated with the fast photolysis of the complexes of by-products anchored at the surface $\equiv Fe^{3+}$, e.g., by a reaction similar to (8) for final carboxylates. The parallel treatment with a WWTP effluent reduced the mineralization power of the system to 67% of COD and 63% of TOC, values acceptable for practical application.

dos Santon et al. (2020) proved the use of sodium vermiculite (an iron-rich clay mineral) as a solid iron catalyst to remove the dye Ponceau SS. The cell was like Fig. 1a equipped with a BDD anode and a carbon-PTFE air-diffusion cathode submitted to a 6 W UVA light or direct sunlight. It was filled with 130 mL of 0.075–0.225 mM dye in pure water by adding 0.050 M Na_2SO_4 and 0.25–2 g L^{-1} catalyst at pH = 3.0, 25 °C, and $j = 16.6$–66.6 mA cm^{-2} lasting 360 min. The catalyst was able to efficiently produce heterogeneous BDD($^{\bullet}OH$) as well as $^{\bullet}OH$ from reaction (10) and similar to reaction (7) with surface $\equiv Fe^{3+}$ to largely oxidize the dye and its by-products, whose surface $\equiv$ Fe(III) complexes were rapidly photolyzed. So, a k_{dis} = 0.0123 min^{-1} with 77% TOC removal and 6.1% MCE was obtained with UVA light, which was upgraded using sunlight up to 0.0140 min^{-1}, 84%, and 6.4%,

Table 2
Selected results were obtained for heterogeneous PEF and hybrid and sequential treatments of organic pollutants in different aqueous matrices.

System	Pollutant	Experimental remarks	Main results	Ref.
Heterogeneous PEF				
Fig. S8, BDD anode, carbon felt cathode, air injection, Fe/TiO_2/perlite catalyst 2500 lm UVA-LED lamp	1-butyl-2,3-dimethylimidazolium	320 mL of 25 mg L^{-1} chemical in pure water and WWTP effluent, 0.010 M Na_2SO_4, 2.72 g L^{-1} catalyst, natural pH, 20 °C, I = 50 mA, 240 min	Overall removal in 120 min, more rapidly than simpler combinations of the catalyst. COD and TOC reduction: 80% and 70% in pure water >67% and 63% in WWTP	Diez et al. (2020)
Like Fig. 1a, BDD anode, carbon-PTFE air-diffusion cathode, sodium vermiculite catalyst, 6 W UVA light, sunlight	Ponceau SS	130 mL of 0.075–0.225 mM dye in pure water, 0.050 M Na_2SO_4, 0.25–2 g L^{-1} catalyst, pH = 3.0, 25 °C, j = 16.6–66.6 mA cm^{-2}, 360 min	For 0.150 mM dye, 1 g L^{-1} catalyst, and j = 33.3 mA cm^{-2}, k_{dis} (min^{-1}), TOC decay, and MCE: 0.0123, 77% and 6.1% for UVA and 0.0140, 84%, and 6.4% for sunlight. Evolution of 5 carboxylic acids by HPLC	dos Santos et al. (2020)
Stirred tank reactor with a 500 W Xe lamp (cut-off of λ > 420 nm), BDD anode, MOFs (2Fe/Co)/carbon fiber cathode, SCE reference electrode, O_2 injection	Methylene Blue Erythromycin	100 mL of 50 mg L^{-1} dye or 50 mg L^{-1} drug in pure water, 20 mg L^{-1} Na_2SO_4, pH = 3.0, room temperature, E_{cat} [b] = −1.0 V/SCE, 60 min	Discoloration and TOC removal: 98% and 95% for Methylene Blue and 98% and 92% for Erythromycin. $^{\bullet}OH$ as the main oxidant. For the latter dye, excellent reusability after 5 consecutive cycles	Li et al. (2023a)
Hybrid				
Like Fig. 1a with a 5 W UVC lamp at the bottom, Ti/RuO_2 anode, air-diffusion cathode, FeCu/porous carbon photocatalyst	Sulfamethazine	200 mL of 10–80 mg L^{-1} drug in pure water, 0.050 M Na_2SO_4, 5–35 mg L^{-1} photocatalyst, pH = 3.0–7.0, room temperature, I = 5–35 mA, 60 min	Total decay in 40 min for 80 mg L^{-1} drug, 25 mg L^{-1} photocatalyst, pH = 4.0, and I = 25 mA. Leaching of Fe and Cu. $^{\bullet}OH$ and $O_2^{\bullet-}$ oxidants detected by EPR. Excellent reusability after 5 successive steps. Evolution of 5 carboxylic acids by HPLC	Du et al. (2022)
Stirred tank reactor with an inner 500 W Xe lamp, Pt anode, FeS_2 NWs [a]/Ti_3C_2 photocathode, O_2 injection	Sulfamethazine	100 mL of 5 and 10 mg L^{-1} drug in pure water, 0.050 M Na_2SO_4, 5–9 mg cm^{-2} photocatalyst onto the cathode, pH = 3.0–9.0, room temperature, I = 100–300 mA, 100 min	Complete abatement for 5 mg L^{-1} drug, 7 mg cm^{-2} catalyst, pH = 3.0–7.0, and I = 200 mA. Good reusability with loss of 9% degradation after 5 consecutive steps	Xia et al. (2021)
Stirred tank reactor with an inner 10 W LED (λ = 520 nm) lamp, Cu anode, graphite cathode, TiO_2/glycine/$ZnFe_2O_4$ photocatalyst, O_2 injection	Acid Black 172 Reactive Blue 19	500 mL of 50–200 mg L^{-1} dye in pure water, 0.050 M Na_2SO_4, 1 g L^{-1} photocatalyst, pH = 4.0–8.0, 25 °C, j = 2–6 mA cm^{-2}, 90 min	Optimized discoloration by response surface methodology for suspended or immobilized at the cathode photocatalyst: 72% and 92% for Acid Black 172 at pH = 6,5, j = 2 mA cm^{-2}, and 48 min, 80% and 95% for Reactive Blue 19 at pH = 6,5, j = 2.7 mA cm^{-2}, and 30 min	Aflaki et al. (2021)
Fig. 4a with a FTO [c]/TiO_2 photoanode upon a 0.05 mWm^{-2} UVA lamp, a carbon felt cathode, and an Ag|AgCl electrode reference, O_2 injection	Triphenyltin chloride	50 mL of 0.1 mM chemical in pure water, 0.050 M K_2SO_4, 0.2 mM Fe^{2+}, pH = 3.0, room temperature, E_{an} = +2.5 V/Ag|AgCl, 360 min	96% (k_1 = 0.219 min^{-1}) removal by PEF and 98% (k_1 = 0.274 min^{-1}) by PEF/PEC in 60 min, respectively. Total TOC reduction in 120 min by PEF/PEC and 360 min by PEF. 10 aromatic, 3 cyclic, and 5 carboxylic acids by-products identified by LC-MS/MS and HPLC	Xu et al. (2020)
Stirred tank reactor with a blue-TiO_2 nanotube array photoanode upon a 200 W Xe lamp, a carbon felt cathode, and an SCE electrode reference, O_2 injection	2,4-Dichlorophenoxyacetic acid	100 mL of 5–20 mM herbicide in pure water, 0.050 M Na_2SO_4, 0–0.3 mM Fe^{2+}, pH = 1.5, room temperature, E_{an} = from 0 to +2.8 V/SCE, 60 min	Complete abatement in 60 min for 10 mM herbicide, 0.2 mM Fe^{2+}, and E_{an} = +2.4 V/SCE. $^{\bullet}OH$ is the main oxidant	Zhang et al. (2021)
Sequential				
Electrocoagulation with two parallel Fe electrodes (Fig. 5a) followed by PEF-like with a Ti/Ir–Sn–Sb oxide anode and a stainless-steel cathode exposed to a 15 W UVA lamp (Fig. 5c)	Acid Blue 29	Electrocoagulation: 2 L of 500 mg L^{-1} of COD of the dye in pure water, 2 kg NaCl, pH = 7.3, 25 °C, j = 14 mA cm^{-2}, flow velocity = 0.69 cm s^{-1}, 180 min. PEF-like: 0.4 mM Fe^{2+}. pH = 3.0, j = 15 mA cm^{-2}, flow velocity = 24.2 cm s^{-1}, 420 min.	Second electrocoagulation: 94% color removal and 49% COD decay in 180 min. Further PEF-like process with Fe^{2+}: 100% color removal and 98% COD decay in 420 min	Marquez et al. (2022a)
Like Fig. 1c. Electroactivated persulfate with a Ti/RuO_2 anode, graphite felt air-diffusion cathode, followed by PEF with UVA light	Reactive Orange 16	2 L of 30–50 mg L^{-1} TOC_0 of the dye in pure water, 0.050 M Na_2SO_4, first 0.5–1.6 mM PS [d] followed by 0.5 mM Fe^{2+} for PEF, pH = 3.0–9.0, 25 °C, liquid flow rate = 0.5–2 L min^{-1}, j = 5–30 mA cm^{-2}, 360 min each step	First step with PS: 37% TOC reduction for 50 mg L^{-1} TOC_0 at 1 mM PS, pH = 3.0, liquid flow rate = 1 L min^{-1}, and j = 10 mA cm^{-2}. Post-PEF: 98% mineralization with 30% MCE and EC_{TOC} = 0.060 kWh (g TOC)$^{-1}$ under the same conditions. Total operating cost (including UVA lamp): 25.9 US$ m^{-3}. Evolution of 6 carboxylic acids by HPLC and NH_4^+	Cornejo et al. (2023a)

[a] NWs: Nanowires.
[b] E_{cat}: Cathodic potential.
[c] FTO: Fluoride-doped tin oxide. [d] E_{an} = Anodic potential.
[d] PS: Persulfate.

respectively (see Table 2). The authors also followed the evolution of 5 final carboxylic acids by HPLC.

Metal-organic frameworks (MOFs) are porous polymers with metal-clusters coordinated to organic ligands yielding 1D, 2D, or 3D structures of high stability. The use of MOF catalysts as cathodes for heterogeneous PEF should be a hot research line in next future. The good performance of these catalysts has been checked for Methylene Blue and Erythromycin operating with a stirred three-electrode cell equipped with a BDD anode, a MOFs (2Fe/Co)/carbon fiber cathode, and a SCE reference electrode (Li et al., 2023a). The cell was submitted to a 500 W Xe lamp with a cut-off of λ > 420 nm, thus providing visible light. It was filled with 100 mL of 50 mg L^{-1} of each pollutant in pure water with 20 mg L^{-1} Na_2SO_4 at pH = 3.0 and room temperature, which was electrolyzed by applying a cathodic potential (E_{cat}) of −1.0 V/SCE that gave

sufficient H_2O_2 production. More than 92% of each compound and TOC were reduced after 60 min of electrolysis (see Table 2). It was found that $^{\bullet}OH$ was the main oxidant, which proceeded from BDD($^{\bullet}OH$) and heterogeneous $^{\bullet}OH$ formed from the reaction of H_2O_2 with $\equiv Fe^{2+}$ by heterogeneous Fenton reaction (10) and a similar reaction of $\equiv Co^{2+}$ leading to $\equiv Co^{3+}$. The visible light enhanced the mineralization under the action of surface reactions similar to (7) and (8). The excellent performance found for the cathode encourages further studies to confirm its viability in the pilot plant, which is supported by its excellent reusability obtained after 5 consecutive cycles of erythromycin degradation.

9. Combined processes

Several hybrid and sequential processes have been proposed as combined treatments with PEF. Hybrid processes involve the coupling with PC or PEC, whereas sequential ones with EC and PS. Table 2 shows the selected results for these treatments.

9.1. Hybrid processes

PEF/PC treatments have been described for the dyes Acid Black 172 and Reactive Blue 19 (Aflaki et al., 2021) and the drugs bezafibrate (Ye et al., 2020b), carbamazepine (Liu et al., 2024), ciprofloxacin (Bai et al., 2019), and sulfamethazine (Xia et al., 2021; Du et al., 2022). PEF/PEC processes have been developed for the chemical triphenyltin chloride (Xu et al., 2020), the herbicides 2,4-D (Zhang et al., 2021) and simazine (Xu et al., 2021), and the drug paracetamol (Olvera-Rodriguez et al., 2019). Thor et al. (2021, 2023) have reported the coupling of a PEF system with a PEC fuel cell.

PC consists of the light irradiation of a semiconductor material to photoexcite the electrons from its VB to its CB, separated by a band gap energy (E_g), according to reaction (25) (see Fig. S9b). The energy of photons has to be $\geq E_g$ and so, photoinduced e^-_{CB}/h^+_{VB} pairs with the electron at the CB (e^-_{CB}), and positive hole at the VB (h^+_{VB}) are formed (Brillas and Garcia-Segura, 2023). h^+_{VB} is a strong oxidant that directly attacks organics or reacts with H_2O to give $^{\bullet}OH$ from the reaction (26). In contrast, e^-_{CB} is a strong reductant yielding $O_2^{\bullet-}$ and $^{\bullet}OH$ by reactions (27) and (28), respectively. The fast recombination of both photogenerated species from reaction (29) is the main drawback of PC.

$$\text{Semiconductor} + h\nu \rightarrow e^-_{CB} + h^+_{VB} \quad (25)$$

$$h^+_{VB} + H_2O \rightarrow {}^{\bullet}OH + H^+ \quad (26)$$

$$e^-_{CB} + O_2 \rightarrow O_2^{\bullet-} \quad (27)$$

$$e^-_{CB} + H_2O_2 \rightarrow {}^{\bullet}OH + OH^- \quad (28)$$

$$e^-_{CB} + h^+_{VB} \rightarrow \text{Semiconductor} + \text{heat} \quad (29)$$

Du et al. (2022) reported the removal of sulfamethazine with a suspended FeCu/porous carbon photocatalyst using a stirred tank reactor like Fig. 1a with a Ti/RuO_2 anode and an air-diffusion cathode, with the variant of putting a 5 W UVC lamp at its bottom. The complex PEF/PC mechanism of Fig. S9a was proposed to explain the generation of oxidants. It considered that the photocatalyst contained Fe_3O_4 and CuO that generate e^-_{CB} from reaction (25) and its surface $\equiv Fe^{2+}$ and $\equiv Cu^+$ species can produce heterogeneous oxidant $^{\bullet}OH$ from Fenton's-like reactions (10) and (30), respectively. The photoinduced e^-_{CB} can then reduce O_2 to $O_2^{\bullet-}$ from reaction (27) and H_2O_2 to $^{\bullet}OH$ from reaction (28). This last process also occurs through reaction (9) under UVC light. Moreover, Fe and Cu were leached to the medium, opening a homogeneous oxidation way. Apart from O_2 reduction to H_2O_2 by reaction (1), soluble Fe^{3+} and Cu^{2+} can be reduced to Fe^{2+} and Cu^+ through reactions (6) and (31), respectively, so that, homogeneous $^{\bullet}OH$ can also be formed from Fenton's reaction (5) and Fenton-like reaction (32). The photolysis of $Fe(OH)^{2+}$ by reaction (7) and $Fe(OOCR)^{2+}$ by reaction (8) finally leads to higher mineralization.

$$\equiv Cu^+ + H_2O_2 \rightarrow \equiv Cu^{2+} + {}^{\bullet}OH + OH^- \quad (30)$$

$$Cu^{2+} + e^- \rightarrow Cu^+ \quad (31)$$

$$Cu^+ + H_2O_2 \rightarrow Cu^{2+} + {}^{\bullet}OH + OH^- \quad (32)$$

Total drug removal was found after 40 min of electrolysis of 200 mL of 80 mg L^{-1} drug in pure water with 0.050 M Na_2SO_4 and 25 mg L^{-1} photocatalyst at pH = 4.0, room temperature, and I = 25 mA (see Table 2). It is noticeable that the generation of $^{\bullet}OH$ and $O_2^{\bullet-}$ as oxidants were detected by EPR by the complex formed with 5,5-dimethyl-1-pyrroline N-oxide (DMPO). An excellent reusability of the photocatalyst was determined after 5 successive steps. The evolution of 5 final carboxylic acids was followed by HPLC.

A slower degradation of sulfamethazine has been reported by Xia et al. (2021) using a stirred tank reactor with a Pt anode, a FeS_2 nanowires (NWs)/Ti_3C_2 photocathode, and an inner 500 W Xe light simulating sunlight. Fig. S9b presents the mechanism proposed for this PEF/PC system. H_2O is oxidized at the Pt surface to form Pt($^{\bullet}OH$) from reaction (3). The FeS_2 NWs produce photoinduced e^-_{CB} under visible irradiation from the reaction (25). These electrons can reduce: (i) O_2 to H_2O_2 by reaction (1), (ii) H_2O_2 to heterogeneous $^{\bullet}OH$ from reaction (28), and (iii) $\equiv Fe^{3+}$ to $\equiv Fe^{2+}$ by a reaction similar to (6) to produce more heterogeneous $^{\bullet}OH$ and accelerate the heterogeneous Fenton reaction (10). Photolysis of $\equiv Fe^{3+}$ species by a reaction similar to (7) also contributes to $\equiv Fe^{2+}$ regeneration. Oxidation of SO_4^{2-} from the electrolyte yields the strong oxidant $SO_4^{\bullet-}$, although heterogeneous $^{\bullet}OH$ is the main oxidant of sulfamethazine and its by-products. PEF/PC trials performed with 100 mL of 5 and 10 mg L^{-1} drug in pure water, 0.050 M Na_2SO_4, and 5–9 mg cm^{-2} catalyst onto the cathode at pH = 3.0–9.0, room temperature, and I = 100–300 mA revealed a slower degradation rate than the above reported by Du et al. (2022). So, 100 min were required for the overall removal of 5 mg L^{-1} drug with 7 mg cm^{-2} catalyst at pH = 3.0–7.0 and I = 200 mA (see Table 2). The cathode presented a good reusability with a loss of 9% degradation after 5 consecutive steps.

Aflaki et al. (2021) checked the performance of the hybrid PEF/PC treatments of Acid Black 172 and Reactive Blue 19 using suspended or cathodically immobilized TiO_2/glycine/$ZnFe_2O_4$ photocatalyst. Response surface methodology was applied to optimize the treatment of 500 mL of 50–200 mg L^{-1} of each dye in pure water by adding 0.050 M Na_2SO_4 and 1 g L^{-1} photocatalyst at pH = 4.0–8.0, 25 °C, and j = 2–6 mA cm^{-2}. The best results were obtained at pH = 6.5 for both suspended and immobilized photocatalysts, with discoloration efficiencies of 72% and 92% for Acid Black 172 at j = 2 mA cm^{-2} and 48 min, and 80% and 95% for Reactive Blue 19, at j = 2.7 mA cm^{-2} and 30 min (see Table 2). These findings point to consider that immobilized photocatalysts at the cathode are preferable to be used against suspended ones in practice, although more comparative research is needed to confirm this suggestion.

PEC consists of the use of a photoanode that is irradiated to yield the generation of oxidizing species from reactions (25)–(28), with minimization of reaction (29) due to the pass of the photoinduced e^-_{CB} to the cathode through the external electric circuit. Fig. 4a shows a sketch of the simple three-electrode photoelectrolytic cell for the PEF/PEC process with a fluoride-doped tin oxide (FTO)/TiO_2 photoanode directly illuminated with 0.05 mW m^{-2} UVA lamp (Xu et al., 2020). The cathode was a Pt/carbon felt and the reference electrode was an Ag|AgCl. With this system, 50 mL of 0.1 mM of the chemical triphenyltin chloride in pure water with 0.050 M K_2SO_4 and 0.2 mM Fe^{2+} at pH = 3.0 and room temperature were remediated by applying an anodic potential (E_{an}) of +2.5 V/Ag|AgCl lasting 360 min. The comparative normalized chemical concentration and TOC decay using FTO/TiO_2 without illumination, PEC, PEF, and PEF/PEC are presented in Fig. 4b and c, respectively. The inset of Fig. 4b highlights the good pseudo-first-order kinetic analysis

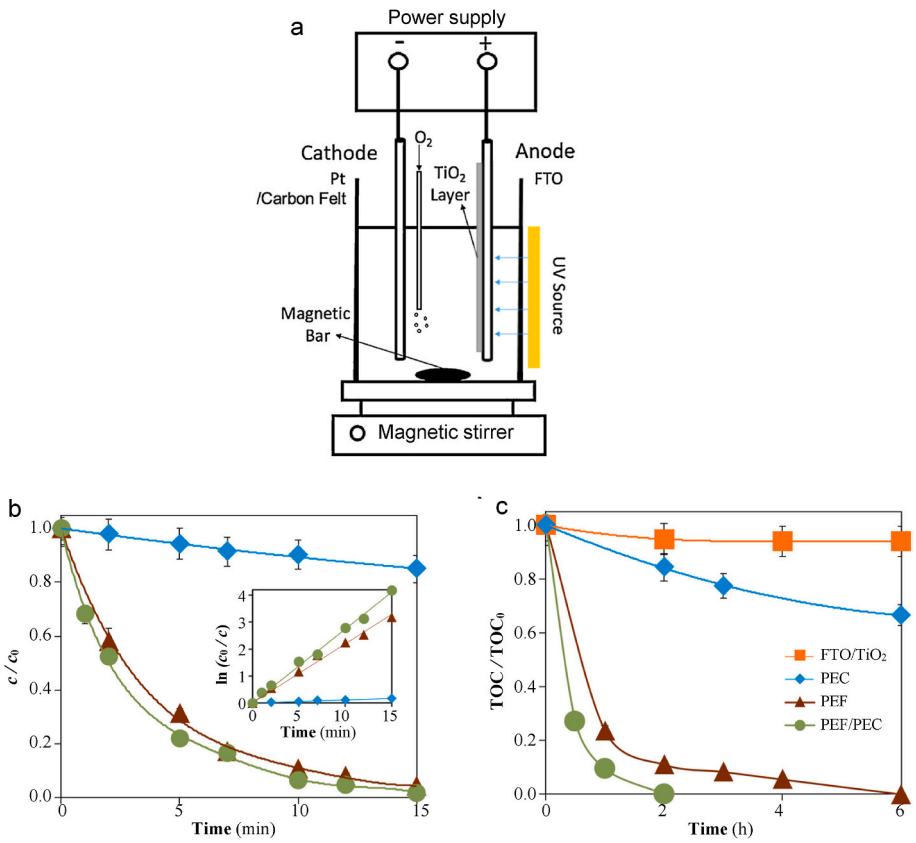

Fig. 4. (a) Schematic representation of the photoelectrolytic cell used for the hybrid PEF/photoelectrocatalysis (PEC) process with an FTO/TiO_2 photoanode upon a 0.05 mWm^{-2} UVA lamp and a carbon felt cathode. An Ag|AgCl electrode reference was added for the assays. Normalized (b) triphenyltin chloride concentration and (c) TOC with time for 50 mL of 0.1 mM chemical (20 mg L^{-1} TOC_0) in pure water with 0.050 M K_2SO_4 and 0.2 mM Fe^{2+} at pH = 3.0, room temperature, and an anodic potential (E_{an}) of +2.5 V/Ag|AgCl for different processes. The inset panel of (b) presents the pseudo-first-order kinetic analysis of the corresponding concentration decays. Adapted from Xu et al. (2020).

found for the corresponding concentration decays. As can be seen, the best process was PEF/PEC yielding 98% degradation with $k_1 = 0.274$ min^{-1} in 60 min and total TOC reduction in 120 min. It upgraded the PEF process that gave 96% degradation with $k_1 = 0.219$ min^{-1} in 60 min and total TOC abatement in 360 min (see Table 2). From the by-products identified for the PEF/PEC process by LC-MS/MS and HPLC, indicating the main oxidative action of generated $^{\bullet}OH$, the proposed reaction mineralization sequence for triphenyltin chloride (**1**) is depicted in Fig. S10. This chemical presents two reactive sites, the high electron density in the aromatic moieties and the highly polar Sn–C center. The process was then initiated by the introduction of –OH groups over the benzenic rings to form the dihydroxylated **2** and the monohydroxylated **3**. Further attack of O_2 yielding $O_2^{\bullet-}$ causes the loss of one hydroxylated benzene of both by-products to form **4** and **5**. The same reaction over **5** originates **6** is hydroxylated to **7**, followed by the loss of Sn^{4+} and Cl^- to form phenol (**8**). Subsequent hydroxylation of **8** yields hydroquinone (**9**) and catechol (**10**) that are oxidized to 1,4-benzoquinone (**11**) and 1, 2-benzoquinone (**12**), respectively. The ring cleavage of these compounds leads to maleic (**13**) and fumaric (**14**) acids, which are oxidized to glycolic acid (**15**). The latter is finally transformed into the ultimate oxalic (**16**) and formic (**17**) acids that are directly converted into CO_2. Note that these 5 carboxylic acids are complexed with Fe^{3+} in solution and quicky photodecarboxylated by reaction (8), thus explaining the fast and total mineralization achieved for triphenyltin chloride by PEF/PEC.

Zhang et al. (2021) also reported the generation of $^{\bullet}OH$ as the main oxidant for an efficient PEF/PEC process of 2,4-D. They used a stirred tank reactor with a blue-TiO_2 nanotube array photoanode upon a 200 W Xe lamp, a carbon felt cathode, and an SCE electrode reference. Complete degradation was obtained after 60 min of electrolysis of 100 mL of 10 mM herbicide in pure water containing 0.050 M Na_2SO_4 and 0.2 mM Fe^{2+} at pH = 1.5 and room temperature upon application of E_{an} = +2.4 V/SCE (see Table 2).

9.2. Sequential processes

Sequential processes including EC-PEF for the dyes Acid Blue 112, Acid Blue 29, and Brilliant Green (Marquez et al., 2022a, 2022b, 2023) and PS-PEF for the dye Reactive Orange 16 (Cornejo et al., 2023a) have been developed. A complex treatment train with H_2O_2 oxidation, chemical precipitation, biological oxidation, chemical coagulation with $FeCl_3$, and homogeneous PEF-UVA has been checked for textile wastewater (Silva et al., 2020) and industrial waste landfill leachate (Segundo et al., 2020).

EC is based on the solubilization of a Fe anode to $Fe^{2+}$from reaction (20), followed by its precipitation as $Fe(OH)_{2(s)}$ from reaction (33) or its oxidation with O_2 to form $Fe(OH)_{3(s)}$ from reaction (34).

$$Fe^{2+} + 2\ OH^- \rightarrow Fe(OH)_{2(s)} \quad (33)$$

$$4\ Fe^{2+} + 10H_2O + O_2 \rightarrow 4\ Fe(OH)_{3(s)} + 8\ H^+ \quad (34)$$

$Fe(OH)_{2(s)}$ and $Fe(OH)_{2(s)}$are coagulants/flocculants that can adsorb dyes, micelles, colloids, and other charged pollutants from the wastewater to separate them by sedimentation. The main drawbacks of this procedure are (i) anode passivation and sludge deposition on the electrodes and (ii) generation of iron ions that can be partially dissolved in the final solution, although they can catalyze a further PEF post-treatment (Brillas, 2020).

Marquez et al. (2022a) designed the sequential EC-PEF-like system

schematized in Fig. 5a–d. Fig. 5a presents the up-flow parallel plate EC reactor with a Fe/Fe cell and Fig. 5b the pre-pilot plant for the EC process. This was carried out with 2 L of 500 mg L^{-1} of COD of Acid Blue 29 dye by adding 2 kg NaCl at pH = 7.3, 25 °C, and flow velocity = 0.69 cm s^{-1} by applying a j = 14 mA cm^{-2} for 180 min. Apart from the generation of $Fe(OH)_{2(s)}$ and $Fe(OH)_{3(s)}$ as coagulants/flocculants, the presence of Cl^-originated active chlorine (HClO, ClO^-) from reactions (12)–(14) that oxidize the dye and its by-products. Fig. 5c shows the flow-by filter-press reactor equipped with a Ti/Ir–Sn–Sb oxide anode and a stainless-steel cathode upon a 15 W UVA light for homogeneous PEF-like and Fig. 5d shows the pre-pilot plant used. This process was made without and with the addition of 0.4 mM Fe^{2+} at pH = 3.0 and flow velocity = 24.2 cm s^{-1} by applying a j = 15 mA cm^{-2} during 420 min. In this process, M($^{\bullet}$OH) and active chlorine were formed at the anode, and in the presence of Fe^{2+} (PEF-like + Fe^{2+}), homogeneous $^{\bullet}$OH was produced from reaction (24) as well. Fig. 5e discloses that 94% of

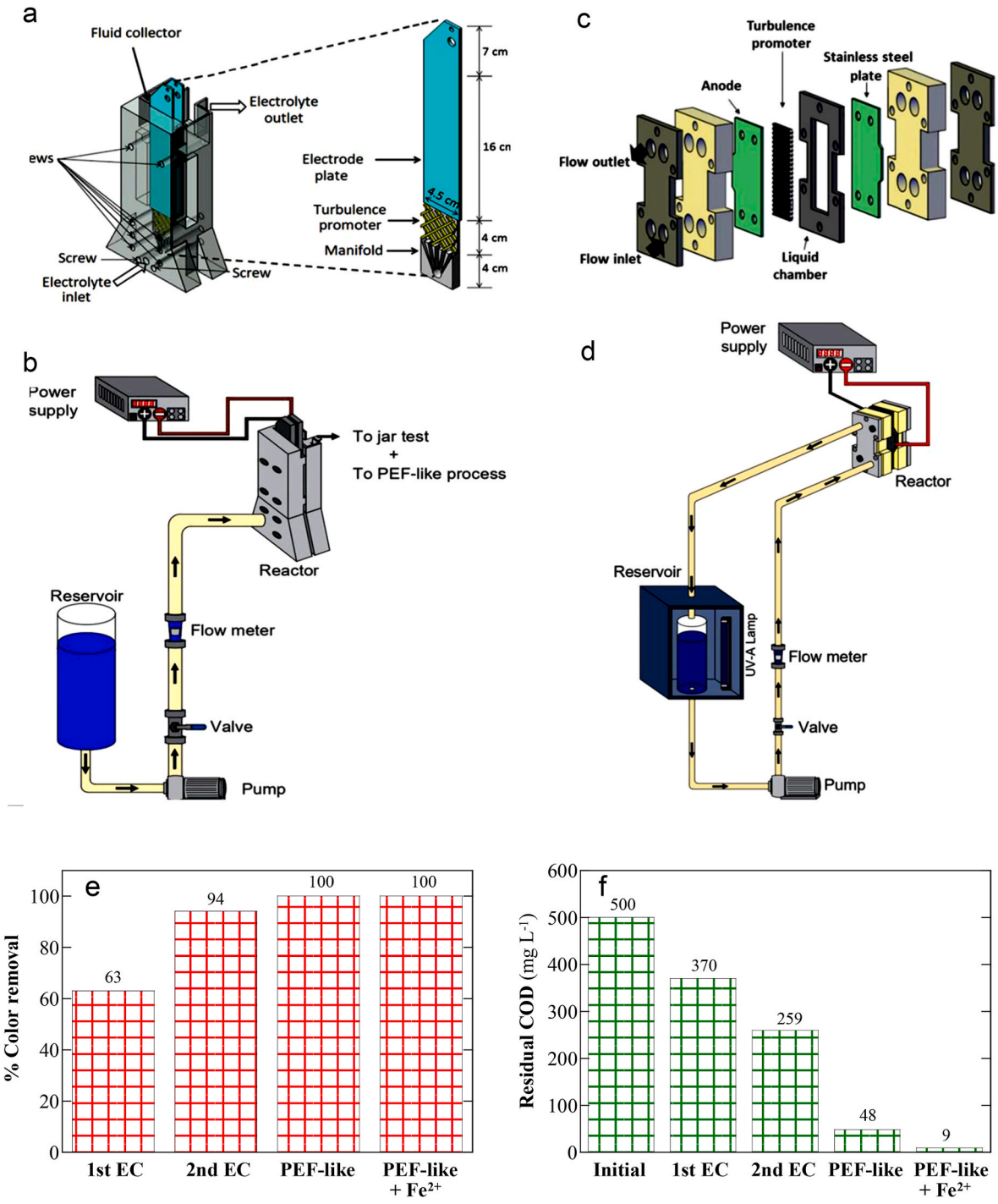

Fig. 5. (a) Up-flow parallel plate electrocoagulation (EC) reactor with a Fe/Fe cell and (b) scheme of the pre-pilot plant for the EC process. (c) Exploded view of the electrochemical filter-press reactor with a Ti/Ir–Sn–Sb oxide anode and a stainless-steel cathode exposed to a 15 W UVA lamp and (d) sketch of the pre-pilot plant for the PEF-like process. (e) Percentage of color removal and (f) residual COD for different processes involving the EC process of 2 L of 500 mg L^{-1} of COD of Acid Blue 29 dye with 2 kg NaCl at pH = 7.3, 25 °C, and flow velocity = 0.69 cm s^{-1} by applying a j = 14 mA cm^{-2} for 180 min. The subsequent PEF-like was made by adding 0.4 mM Fe^{2+} at pH = 3.0 and flow velocity = 24.2 cm s^{-1} by applying a j = 15 mA cm^{-2} during 420 min. Adapted from Marquez et al. (2022a).

color was removed after 2 consecutive EC steps, whereas total discoloration was reached after both, PEF-like and PEF-like + Fe^{2+} treatments (see Table 2). From Fig. 5f, one can infer that the initial 500 mg L^{-1} of COD of the wastewater was reduced by 49% in the second consecutive EC step, which raised to 92% after PEF-like and a satisfactory 98% after PEF-like + Fe^{2+}. The addition of 0.4 mM Fe^{2+} in the latter case enhanced the formation of final Fe(III)-carboxylate complexes that were more quickly photolyzed by UVA light. The authors calculated an operating cost of the sequential EC-PEF-like of 1.36–1.39 US$ m^{-3}, without considering the high cost of the electrical energy provided to the UVA lamp, thus opening the door to further study the alternative use of more cost-effective SPEF-like post-treatment for practical application.

A recent work of Cornejo et al. (2023a) proposed a novel sequential PS-PEF process for the mineralization of Reactive Orange 16 with a flow system like Fig. 1c with a Ti/RuO_2 anode and a graphite felt air-diffusion cathode. The electroactivation of PS was performed in the dark by its reaction with electrogenerated H_2O_2 to form $SO_4^{\bullet-}$ and $^{\bullet}OH$ following reaction (35). $SO_4^{\bullet-}$ can then be hydrolyzed to produce more $^{\bullet}OH$ by reaction (36). However, this treatment was not powerful enough, and only 37% of TOC was reduced starting from 2 L of 50 mg L^{-1} TOC_0 in pure water with 0.050 M Na_2SO_4, and 1 mM PS at pH = 3.0, liquid flow rate = 1 L min^{-1}, and j = 10 mA cm^{-2} (see Table 2). The formation of stable carboxylic acids inhibited the mineralization process.

$$S_2O_8^{2-} + H_2O_2 \rightarrow 2SO_4^{\bullet-} + 2^{\bullet}OH \quad (35)$$

$$SO_4^{\bullet-} + H_2O \rightarrow SO_4^{2-} + {}^{\bullet}OH + H^+ \quad (36)$$

Subsequent homogeneous PEF treatment of the resulting wastewater was carried out under the same conditions after adding 0.5 mM Fe^{2+} and bu applying a UVA irradiation. For this procedure, excellent results were obtained yielding 98% mineralization with 30% MCE and EC_{TOC} = 0.060 kWh (g TOC)$^{-1}$, indicating its feasible viability in practice. In this case, the rapid disappearance of 6 final carboxylic acids was followed by HPLC due to the fast photodecarboxylation of its Fe(III) complexes by reaction (8). Total operating costs were also calculated including that of the UVA lamp giving rise to a value as high as 25.9 US$ m^{-3}, pointing again to the study of the irradiation with sunlight to offer a much more cost-effective PS-PEF process that can be much more attractive at industrial scale.

10. Conclusions and prospects

The results summarized in this review suggest that future research should be centered on the development of homogeneous, heterogeneous, and combined processes with SPEF, especially for the remediation of textile and pharmaceutical industries' wastewaters, as well as urban effluents as tertiary treatment. The use of sunlight in SPEF makes it a more cost-effective effective and viable process than PEF with UV light. However, since SPEF only runs in the daily hours of the sun, integrated systems with UV light irradiation could be coupled to continuous operation in the dark. So, autonomous systems with integrated photovoltaic/PEF/SPEF systems could be designed and tested to prevent the consumption of external electrical energy, an interesting option for industrial applications. A larger area would be occupied by solar photovoltaic panels, becoming space a key issue issue for its implementation. Operating variables should be optimized. The MCE decay at low organic load needs to be clarified to more efficiently remediate urban wastewater with micropollutants. For each anode/cathode pair, the rate of accumulated H_2O_2 and Fe^{2+} regeneration has to be assessed to understand their performance, and the best configuration of the cell and optimum electrodes should be well-defined for the faster destruction of pollutants. Cleaning protocols of the cell, electrodes, and external devices have to be well established to maintain the performance for long-term application. For PEF, the irradiance of the UV lamp should be optimized and controlled to minimize its energy cost. Better solar photoreactors with maximum capture of photons from sunlight also need to be developed for SPEF, making possible their industrial applicability.

High efficiency has been found for emerging homogeneous EF, PEF, and SPEF in removing toxic and recalcitrant industrial chemicals, herbicides, dyes, and drugs in a sulfate medium at pH = 3.0 because of the large formation of homogeneous $^{\bullet}OH$ from Fenton's reaction. The mineralization in homogeneous PEF and SPEF was enhanced by the photolysis of the final Fe(III)-carboxylate species. Better results were obtained in PEF with UVC light that photolyzed H_2O_2 to $^{\bullet}OH$. In chloride media, active chlorine accelerated the degradation of the target pollutant but produced recalcitrant chloroderivatives that slowed down its mineralization. PEF and SPEF processes were also very effective for real wastewater with DSA anodes because they generate more active chlorine than BDD. Overall operating costs for phenol abatement showed that EF was more cost-effective than PEF due to the high cost of the UVA lamp. More techno-economic studies with cost evaluation should be made in the future to confirm this behavior, which can open the door to applying the homogeneous SPEF in practice.

The stabilization of Fe^{3+} by its quenching with EDDS offered a novel and interesting approach to operate with a powerful homogeneous PEF-like, allowing the use of BDD and cheaper DSA anodes at pH = 7.0. However, the addition of this organic difficult its mineralization process. Novel homogeneous PEF-HClO and SPEF-HClO processes in chloride medium have been proposed but they were not useful for decontamination by the loss of HClO from its reaction with Fe^{2+}. Among the heterogeneous PEF processes, solid iron catalysts like Fe/TiO_2/perlite and vermiculite were appropriate to remove organics. The application of novel and stable MOFs with Fe, Co, should be extensively studied in the future at a pilot scale under neutral pH and sunlight irradiation for urban and industrial wastewaters to show its potential applicability at the industrial level. FeCu/porous carbon and TiO_2/glycine/$ZnFe_2O_4$ photocatalysts can be used in hybrid PEF/PC processes. The good immobilization of the photocatalyst at the cathode is an important issue that should be explored for exhaustive treatments with novel photocathodes. Homogeneous PEF/PEC with conventional TiO_2 photoanode presented a higher oxidation power up to total mineralization and widely upgraded the PEF process.

CRediT authorship contribution statement

Enric Brillas: Writing – review & editing, Writing – original draft, Supervision, Methodology, Investigation, Conceptualization. **Juan M. Peralta-Hernandez:** Writing – review & editing, Writing – original draft, Methodology, Investigation, Formal analysis, Conceptualization.

Declaration of competing interest

The authors declare that they have no known competing financial interests or personal relationships that could have appeared to influence the work reported in this paper.

Data availability

Data will be made available on request.

Appendix A. Supplementary data

Supplementary data to this article can be found online at https://doi.org/10.1016/j.chemosphere.2024.143465.

References

Aflaki, S., Farhadian, M., Solaimany Nazar, A.R., Tangestaninejad, S., Davari, N., 2021. Investigation of copper plates as anode and TiO_2 glycine/$ZnFe_2O_4$ stabilized on graphite as cathode for textile dyes degradation from aqueous solution under visible light. J. Appl. Electrochem. 51, 1387–1405. https://doi.org/10.1007/s10800-021-01580-y.

Alcaide, F., Alvarez, G., Guelfi, D.R.V., Brillas, E., Sires, I., 2020. A stable CoSP/MWCNTs air-diffusion cathode for the photoelectro-Fenton degradation of organic pollutants at pre-pilot scale. Chem. Eng. J. 379, 122417. https://doi.org/10.1016/j.cej.2019.122417.

An, J., Li, N., Wu, Y., Wang, S., Liao, C., Zhao, Q., Zhou, L., Li, T., Wang, X., Feng, Y., 2020. Revealing decay mechanisms of H_2O_2-based electrochemical advanced oxidation processes after long-term operation for phenol degradation. Environ. Sci. Technol. 54, 10916–10925. https://doi.org/10.1021/acs.est.0c03233.

Antonin, V.S., Aquino, J.M., Silva, B.F., Silva, A.J., Rocha-Filho, R.C., 2019. Comparative study on the degradation of cephalexin by four electrochemical advanced oxidation processes: evolution of oxidation intermediates and antimicrobial activity. Chem. Eng. J. 372, 1104–1112. https://doi.org/10.1016/j.cej.2019.04.185.

Bai, X., Li, Y., Xie, L., Liu, X., Zhan, S., Hu, W., 2019. A novel Fe-free photo-electro-Fenton-like system for enhanced ciprofloxacin degradation: bifunctional Z-scheme WO_3/g-C_3N_4. Environ. Sci.: Nano 848, 113273. https://doi.org/10.1039/c9en00528e.

Barazorda-Ccahuana, H.L., Fajardo, A.S., dos Santos, A.J., Lanza, M.R.V., 2023. Decentralized approach toward organic pollutants removal using UV radiation in combination with H_2O_2-based electrochemical water technologies. Chemosphere 343, 140079. https://doi.org/10.1016/j.chemosphere.2023.140079.

Behfar, R., Davarnejad, R., 2019. Pharmaceutical wastewater treatment using UV-enhanced electro-Fenton process: comparative study. Water Environ. Res. 91, 1526–1536. https://doi.org/10.1002/wer.1153.

Brillas, E., 2020. A review on the photoelectro-Fenton process as efficient electrochemical advanced oxidation for wastewater remediation. Treatment with UV light, sunlight, and coupling with conventional and other photo-assisted advanced technologies. Chemosphere 250, 126198. https://doi.org/10.1016/j.chemosphere.2020.126198.

Brillas, E., Garcia-Segura, S., 2023. Recent progress of applied TiO_2 photoelectrocatalysis for the degradation of organic pollutants in wastewaters. J. Environ. Chem. Eng. 11 (2023), 109635. https://doi.org/10.1016/j.jece.2023.109635.

Brillas, E., Peralta-Hernández, J.M., 2023. Removal of paracetamol (acetaminophen) by photocatalysis and photoelectrocatalysis. A critical review. Sep. Purif. Technol. 309 (2023), 122982. https://doi.org/10.1016/j.seppur.2022.122982.

Bruguera-Casamada, C., Araujo, R.M., Brillas, E., Sires, I., 2019. Advantages of electro-Fenton over electrocoagulation for disinfection of dairy wastewater. Chem. Eng. J. 376, 119975. https://doi.org/10.1016/j.cej.2018.09.136.

Bugueno-Carrasco, S., Monteil, H., Toledo-Neira, C., Sandoval, M.A., Thiam, A., Salazar, R., 2021. Elimination of pharmaceutical pollutants by solar photoelectro-Fenton process in a pilot plant. Environ. Sci. Pollut. Res. 28, 23753–23766. https://doi.org/10.1007/s11356-020-11223-y.

Campos, S., Lorca, J., Vidal, J., Calzadilla, W., Toledo-Neira, C., Aranda, M., Miralles-Cuevas, S., Cabrera-Reina, A., Salazar, R., 2023. Removal of contaminants of emerging concern by solar photo electro-Fenton process in a solar electrochemical raceway pond reactor. Process Saf. Environ. Protect. 169, 660–670. https://doi.org/10.1016/j.psep.2022.11.033.

Chen, T., Jin, G.-P., Xu, Z., Lv, X.-Y., Sun, M., Tian, J.-J., 2022. Improving generation of H_2O_2 and $^{\bullet}OH$ at bismuth hexacyanoferrate/graphene/carbon fibers-based gas diffusion electrode for degradation of dye wastewaters in photo-electro-Fenton process. Int. J. Environ. Sci. Technol. 19, 7941–7950. https://doi.org/10.1007/s13762-021-03533-6.

Clematis, D., Panizza, M., 2021. Electro-Fenton, solar photoelectro-Fenton and UVA photoelectro-Fenton: degradation of Erythrosine B dye solution. Chemosphere 270, 129480. https://doi.org/10.1016/j.chemosphere.2020.129480.

Cornejo, O.M., Pina, F.J., Nava, J.L., 2023a. Hybrid water treatment flow plant using hydrogen peroxide-based electro-activated persulfate and photoelectro-Fenton processes: the combustion of Reactive Orange 16 dye. J. Ind. Eng. Chem. 124, 558–569. https://doi.org/10.1016/j.jiec.2023.05.012.

Cornejo, O.M., Sires, I., Nava, J.L., 2023b. Characterization of a flow-through electrochemical reactor for the degradation of ciprofloxacin by photoelectro-Fenton without external oxygen supply. Chem. Eng. J. 455, 140603. https://doi.org/10.1016/j.cej.2022.140603.

Cornejo, O.M., Sires, I., Nava, J.L., 2023c. Continuous H_2O_2 production sustained by anodic O_2 for the destruction of the antibiotic ampicillin by photoelectro-Fenton process in a rotating cylinder electrode reactor. J. Environ. Chem. Eng. 11, 109326. https://doi.org/10.1016/j.jece.2023.10932.

Corona-Bautista, M., Picos-Benitez, A., Villasenor-Basulto, D., Bandala, E., Peralta-Hernandez, J.M., 2021. Discoloration of azo dye Brown HT using different advanced oxidation processes. Chemosphere 267, 129234. https://doi.org/10.1016/j.chemosphere.2020.129234.

Crispim, A.C., de Araujo, D.M., Martinez-Huitle, C.A., Souza, F.L., Dos Santos, E.V., 2022. Application of electro-Fenton and photoelectro-Fenton processes for the degradation of contaminants in landfill leachate. Environ. Res. 213, 113552. https://doi.org/10.1016/j.envres.2022.113552.

Da Costa Soares, I.C., Oriol, R., Ye, Z., Martinez-Huitle, C.A., Cabot, P.L., Brillas, E., Sires, I., 2021. Photoelectro-Fenton treatment of pesticide triclopyr at neutral pH using Fe(III)-EDDS under UVA light or sunlight. Environ. Sci. Pollut. Res. 28, 23833–23848. https://doi.org/10.1007/s11356-020-11421-8.

Da Costa, A.J.M., Kronka, M.S., Cordeiro-Junior, P.J.M., Fortunato, G.V., dos Santos, A. J., Lanza, M.R.V., 2021. Treatment of Tebuthiuron in synthetic and real wastewater using electrochemical flow-by reactor. J. Electroanal. Chem. 882, 114978. https://doi.org/10.1016/j.jelechem.2021.114978.

da Silva, L.M., Gozzi, F., Cavalcante, R.P., de Oliveira, S.C., Brillas, E., Sires, I., Machulek, Jr.A., 2019. Assessment of 4-aminoantipyrine degradation and mineralization by photoelectro-Fenton with a boron-doped diamond anode: optimization, treatment in municipal secondary effluent, and toxicity. Chemelectrochem 6, 865–875. https://doi.org/10.1002/celc.201801651.

da Silva, V.E.C., Tadayozzi, Y.S., Putti, F.F., Santos, F.A., Forti, J.C., 2022. Degradation of commercial glyphosate-based herbicide via advanced oxidative processes in aqueous media and phytotoxicity evaluation using maize seeds. Sci. Total Environ. 840, 156656. https://doi.org/10.1016/j.scitotenv.2022.156656.

Daniel, G., Zhang, Y., Lanzalaco, S., Brombin, F., Kosmala, T., Granozzi, G., Wang, A., Brillas, E., Sires, I., Durante, C., 2020. Chitosan-derived nitrogen-doped carbon electrocatalyst for a sustainable upgrade of oxygen reduction to hydrogen peroxide in UV-assisted electro-Fenton water treatment. ACS Sustain. Chem. Eng. 8, 14425–14440. https://doi.org/10.1021/acssuschemeng.0c04294.

Deemter, D., Salmeron, I., Oller, I., Amat, A.M., Malato, S., 2022. Valorization of UWWTP effluents for ammonium recovery and MC elimination by advanced AOPs. Sci. Total Environ. 823, 153693. https://doi.org/10.1016/j.scitotenv.2022.153693.

Delgado-Vargas, C.A., Espinosa-Barrera, P.A., Villegas-Guzman, P., Martinez-Pachon, D., Moncayo-Lasso, A., 2022. An efficient simultaneous degradation of sulfamethoxazole and trimethoprim by photoelectro-Fenton process under non-modified pH using a natural citric acid source: study of biodegradability, ecotoxicity, and antibacterial activity. Environ. Sci. Pollut. Res. 29, 42275–42289. https://doi.org/10.1007/s11356-021-17751-5.

Deng, F., Olvera-Vargas, H., Zhou, M., Qiu, S., Sirés, I., Brillas, E., 2023. Critical review on the mechanisms of Fe^{2+} regeneration in the electro-Fenton process: fundamentals and boosting strategies. Chem. Rev. 123, 4635–4662. https://doi.org/10.1021/acs.chemrev.2c00684.

Diez, A.M., Pazos, M., Sanroman, M.A., 2020. Bifunctional floating catalyst for enhancing the synergistic effect of LED-photolysis and electro-Fenton process. Sep. Purif. Technol. 230, 115880. https://doi.org/10.1016/j.seppur.2019.115880.

dos Santos, A.J., Fajardo, A.S., Kronka, M.S., Garcia-Segura, S., Lanza, M.R.V., 2021. Effect of electrochemically-driven technologies on the treatment of endocrine disruptors in synthetic and real urban wastewater. Electrochim. Acta 376, 138034. https://doi.org/10.1016/j.electacta.2021.138034.

dos Santos, A.J., Sires, I., Alves, A.P.M., Martinez-Huitle, C.A., Brillas, E., 2020. Vermiculite as heterogeneous catalyst in electrochemical Fenton-based processes: application to the oxidation of Ponceau SS dye. Chemosphere 240, 124838. https://doi.org/10.1016/j.chemosphere.2019.124838.

dos Santos, P.R., de Oliveira Dourados, M.E., Sires, I., Brillas, E., Cavalcante, R.P., Cavalheri, P.S., Paulo, P.L., Vieira Guelfi, D.R., de Oliveira, S.C., Gozzi, F., Machulek, Jr.A., 2023. Greywater treatment by anodic oxidation, photoelectro-Fenton and solar photoelectro-Fenton processes: influence of relevant parameters and toxicity evolution. Process Saf. Environ. Protect. 169, 879–895. https://doi.org/10.1016/j.psep.2022.11.058.

Droguett, C., Salazar, R., Brillas, E., Sires, I., Carlesi, C., Marco, J.F., Thiam, A., 2020. Treatment of antibiotic cephalexin by heterogeneous electrochemical Fenton-based processes using chalcopyrite as sustainable catalyst. Sci. Total Environ. 740, 140154. https://doi.org/10.1016/j.scitotenv.2020.140154.

Du, X., Su, P., Fu, W., Zhang, Q., Zhou, M., 2022. Heterogeneous photoelectro-Fenton catalyzed by FeCu@PC for efficient degradation of sulfamethazine. Electrochim. Acta 412, 140122. https://doi.org/10.1016/j.electacta.2022.140122.

Duan, Y., Sedlak, D.L., 2024. Electrochemical hydrogen peroxide generation and activation using a dual-cathode flow-through treatment system: enhanced selectivity for contaminant removal by electrostatic repulsión. Environ. Sci. Technol. 58, 14042–14051. https://doi.org/10.1021/acs.est.4c05481.

Echeverry-Gallego, R.A., Espinosa-Barrera, P.A., Delgado-Vargas, C.A., Vanegas, J., Clavijo-Buritic, D.C., Martinez-Pachon, D., Moncayo-Lasso, A., 2023. The application of the photo-electro-Fenton process in the treatment of wastewater reduces the abundance of genes associated with pathogenicity factors, antibiotic resistance, and metabolism: a metagenomic analysis. J. Environ. Chem. Eng. 11, 109937. https://doi.org/10.1016/j.jece.2023.109937.

Esfahani, K.N., Farhadian, M., Nazar, A.R.S., 2019. Interaction effects of various reaction parameters on the treatment of sulfidic spent caustic through electro-photo-Fenton. Int. J. Environ. Sci. Technol. 16, 7165–7174. https://doi.org/10.1007/s13762-018-2126-8.

Ferreira, L.C., Salmeron, I., Peres, J.A., Tavares, P.B., Lucas, M.S., Malato, S., 2020. Advanced Oxidation Processes as sustainable technologies for the reduction of elderberry agro-industrial water impact. Water Resour. Ind. 24, 100137. https://doi.org/10.1016/j.wri.2020.100137.

Forti, J.C., Loretti, G.H., Tadayozzi, Y.S., de Andrade, A.R., 2020. A phytotoxicity assessment of the efficiency 2,4-D degradation by different oxidative processes. J. Environ. Manage. 266, 110588. https://doi.org/10.1016/j.jenvman.2020.110588.

Fortunato, G.V., Kronka, M.S., dos Santos, A.J., Ledendecker, M., Lanza, M.R.V., 2020. Low Pd loadings onto Printex L6: synthesis, characterization and performance towards H_2O_2 generation for electrochemical water treatment technologies. Chemosphere 259, 127523. https://doi.org/10.1016/j.chemosphere.2020.127523.

Gonzaga, I.M.D., Moratalla, A., Eguiluz, Katlin I.B., Salazar-Banda, G.R., Canizares, P., Rodrigo, M.A., Saez, C., 2021. Novel Ti/RuO_2IrO_2 anode to reduce the dangerousness of antibiotic polluted urines by Fenton-based processes. Chemosphere 270, 129344. https://doi.org/10.1016/j.chemosphere.2020.129344.

Herrera-Chavez, S., Pacheco-Alvarez, M., Kadier, A., Brillas, E., Peralta-Hernandez, J.M., 2024. Efficient electrochemical advanced degradation of Red CL and Red WB dyes from the tanning industry using a boron-doped diamond anode. Chemosphere 363, 142825. https://doi.org/10.1016/j.chemosphere.2024.142825.

Khaleel, G.F., Ismail, I., Abbar, A.H., 2023. Application of solar photo-electro-Fenton technology to petroleum refinery wastewater degradation: optimization of operational paràmetres. Heliyon 9, e15062. https://doi.org/10.1016/j.heliyon.2023.e15062.

Kong, J., Huang, W., Yang, S., He, H., Sun, C., Xian, Q., Jiang, D., 2020. Photoelectro-Fenton system including electromagnetic induction electrodeless lamp and black carbon poly tetra fluoro ethylene air-diffusion cathode: degradation kinetics, intermediates and pathway for azo dye. Chemosphere 253, 126708. https://doi.org/10.1016/j.chemosphere.2020.126708.

Kronka, M.S., Fortunato, G.V., Mira, L., dos Santos, A.J., Lanza, M.R.V., 2023. Using Au NPs anchored on ZrO_2/carbon black toward more efficient H_2O_2 electrogeneration in flow-by reactor for carbaryl removal in real wastewater. Chem. Eng. J. 452, 139598. https://doi.org/10.1016/j.cej.2022.139598.

Kronka, M.S., Silva, F.L., Martins, A.S., Almeida, M.O., Honorio, K.M., Lanza, M.R.V., 2020. Tailoring the ORR selectivity for H_2O_2 electrogeneration by modification of Printex L6 carbon with 1,4-naphthoquinone: a theoretical, experimental and environmental application study. Mater. Adv. 1, 1318–1329. https://doi.org/10.1039/d0ma00290a.

Li, B., Meng, Y., Lin, X., Tu, D., Shen, S., He, T., Li, Y., Zhang, H., 2023a. Enhanced photo-electro-Fenton degradation performance using graphene structure-oriented MOFs (2Fe/Co)/CNF cathode membrane. J. Clean. Product. 401, 136782. https://doi.org/10.1016/j.jclepro.2023.136782.

Li, G., Zheng, Y., Hu, G., Chen, B., Gu, Y., Yang, J., Yang, H., Hu, F., Li, C., Guo, C., 2023b. Boosting photo-Electro-Fenton process via atomically dispersed iron sites on graphdiyne for invitro hydrogen peroxide detection. Small 19. https://doi.org/10.1002/smll.202301540.

Liu, C.-F., Huang, C.P., Juang, Y., Hu, C.-C., Huang, C., 2019. Graphite supported stainless-steel electrode for the degradation of azo dye Orange G by Fenton reactions: effect of photo-irradiation. J. Environ. Eng. 145, 04018133. https://doi.org/10.1061/(ASCE)EE.1943-7870.0001476.

Liu, J., Liang, R., Hu, Z., Zhang, X., Zhou, M., 2024. Photoelectrocatalysis/photoelectro-Fenton system based on cone-like TiO_2/nickel foam photoanode for efficient degradation of carbamazepine: comparison with DSA. Chem. Eng. J. 491, 152088. https://doi.org/10.1016/j.cej.2024.152088.

Ma, P., Prestigiacomo, C., Proietto, F., Galia, A., Scialdone, O., 2021. Electrochemical treatment of wastewater by electroFenton, photo-electroFenton, pressurized-electroFenton and pressurized photo electroFenton: a first comparison of these innovative routes. Chemelectrochem 8, 3135–3142. https://doi.org/10.1002/celc.202100736.

Mansour, M.S., Farid, Y., Nosier, S.A., Adli, O., Abdel-Aziz, M.H., 2023. Removal of Eosin Yellow dye from industrial wastewater using UV/H_2O_2 and photoelectro-Fenton techniques. J. Photochem. Photobiol., A: Chem 436, 114411. https://doi.org/10.1016/j.jphotochem.2022.114411.

Marques, Cordeiro-Jr, P, J., Martins, A.S., Santana Pereira, G.B., Rocha, F.V., Rodrigo Rodrigo, M.A., de Vasconcelos Lanza, M.R., 2022. Bisphenol-S removal via photoelectro-Fenton/H_2O_2 process using Co-porphyrin/Printex L6 gas diffusion elèctrode. Sep. Purif. Technol. 285, 120299. https://doi.org/10.1016/j.seppur.2021.120299.

Marquez, A.A., Coreno, O., Nava, J.L., 2022a. A hybrid process combining electrocoagulation and active chlorine-based photoelectro-Fenton-like methods during the removal of Acid Blue 29 dye. J. Electroanal. Chem. 922, 116732. https://doi.org/10.1016/j.jelechem.2022.116732.

Marquez, A.A., Coreno, O., Nava, J.L., 2022b. An innovative process combining electrocoagulation and photoelectro-Fenton-like methods during the abatement of Acid Blue 113 dye. Process Saf. Environ. Protect. 163, 475–486. https://doi.org/10.1016/j.psep.2022.05.061.

Marquez, A.A., Coreno, O., Nava, J.L., 2023. Abatement of a complex mixture of dyes in the presence of chlorides by electrocoagulation and active chlorine-based photoelectro-Fenton-like processes. Process Saf. Environ. Protect. 169, 579–591. https://doi.org/10.1016/j.psep.2022.11.050.

Marquez, A.A., Sires, I., Brillas, E., Nava, J.L., 2020. Mineralization of Methyl Orange azo dye by processes based on H_2O_2 electrogeneration at a 3D-like air-diffusion cathode. Chemosphere 259, 127466. https://doi.org/10.1016/j.chemosphere.2020.127466.

Martínez-Huitle, C.A., Brillas, E., 2021. A critical review over the electrochemical disinfection of bacteria in synthetic and real wastewaters using a boron-doped diamond anode. Curr. Opin. Solid State Mater. Sci. 25, 100926. https://doi.org/10.1016/j.cossms.2021.100926.

Medrano-Rodriguez, F., Picos-Benitez, A., Brillas, E., Bandala, E.R., Perez, T., Peralta-Hernandez, J.M., 2020. Electrochemical advanced oxidation discoloration and removal of three brown diazo dyes used in the tannery industry. J. Electroanal. Chem. 873, 114360. https://doi.org/10.1016/j.jelechem.2020.114360.

Melin, V., Salgado, P., Thiam, A., Henriquez, A., Mansilla, H.D., Yanez, J., Salazar, C., 2021. Study of degradation of amitriptyline antidepressant by different electrochemical advanced oxidation processes. Chemosphere 274, 129683. https://doi.org/10.1016/j.chemosphere.2021.129683.

Mousset, E., Loh, W.H., Lim, W.S., Jarry, L., Wang, Z., Lefebvre, O., 2021. Cost comparison of advanced oxidation processes for wastewater treatment using accumulated oxygen-equivalent criteria. Water Res. 200, 117234. https://doi.org/10.1016/j.watres.2021.117234.

Murrieta, M.F., Brillas, E., Nava, J.L., Sires, I., 2020a. Photo-assisted electrochemical production of HClO and Fe^{2+} as Fenton-like reagents in chloride media for sulfamethoxazole degradation. Sep. Purif. Technol. 250, 117236. https://doi.org/10.1016/j.seppur.2020.117236.

Murrieta, M.F., Brillas, E., Nava, J.L., Sires, I., 2023. Solar photoelectro-Fenton-like process with anodically-generated HClO in a flow reactor: norfloxacin as a pollutant with a particular structure. Sep. Purif. Technol. 308, 122893. https://doi.org/10.1016/j.seppur.2022.122893.

Murrieta, M.F., Sires, I., Brillas, E., Nava, J.L., 2020b. Mineralization of Acid Red 1 azo dye by solar photoelectro-Fenton-like process using electrogenerated HClO and photoregenerated Fe(II). Chemosphere 246, 125697. https://doi.org/10.1016/j.chemosphere.2019.125697.

Nakamura, K.C., Guimaraes, L.S., Magdalena, A.G., Dias Angelo, A.C., De Andrade, A.R., Garcia-Segura, S., Pipi, A.R.F., 2019. Electrochemically-driven mineralization of Reactive Blue 4 cotton dye: on the role of in situ generated oxidants. J. Electroanal. Chem. 840, 415–422. https://doi.org/10.1016/j.jelechem.2019.04.016.

Nidheesh, P.V., Zhou, M., Oturan, M.A., 2018. An overview on the removal of synthetic dyes from water by electrochemical advanced oxidation processes. Chemosphere 197, 210–227. https://doi.org/10.1016/j.chemosphere.2017.12.195.

Olvera-Rodriguez, I., Hernandez, R., Medel, A., Guzman, C., Escobar-Alarcon, L., Brillas, E., Sires, I., Esquivel, K., 2019. TiO_2/Au/TiO_2 multilayer thin-film photoanodes synthesized by pulsed laser deposition for photoelectrochemical degradation of organic pollutants. Sep. Purif. Technol. 224, 189–198. https://doi.org/10.1016/j.seppur.2019.05.020.

Pacheco-Álvarez, M., Picos Benítez, R., Rodríguez-Narváez, O.M., Brillas, E., Peralta-Hernández, J.M., 2022. A critical review on paracetamol removal from different aqueous matrices by Fenton and Fenton-based processes, and their combined methods. Chemosphere 303, 134883. https://doi.org/10.1016/j.chemosphere.2022.134883.

Pacheco-Alvarez, M.O.A., Picos, A., Perez-Segura, T., Peralta-Hernandez, J.M., 2019. Proposal for highly efficient electrochemical discoloration and degradation of azo dyes with parallel arrangement elèctrodes. J. Electroanal. Chem. 838, 195–203. https://doi.org/10.1016/j.jelechem.2019.03.004.

Paz, E.C., Pinheiro, V.S., Sousa Joca, J.F., Sotana de Souza, R.A., Gentil, T.C., Lanza, M.R.V., Moises de Oliveira, H.P., Pereira Neto, A.M., Gaubeur, I., Santos, M.C., 2020. Removal of Orange II (OII) dye by simulated solar photoelectro-Fenton and stability of $WO_{2.72}$/Vulcan XC72 gas diffusion electrode. Chemosphere 239, 124670. https://doi.org/10.1016/j.chemosphere.2019.124670.

Perumal, A., Yesuf, M.B., Govindarajan, R., Niju, S., Arun, C., Periyasamy, S., Pandiyarajan, T., Alemayehu, E., 2023. Photo-alternating current-electro-Fenton process for pollutant removal and energy usage from industrial wastewater: response surface approach optimization of operational parametres. Chemelectrochem 10. https://doi.org/10.1002/celc.202300086.

Pinheiro, A.C.N., Bernardino, T.S., Junior, F.E.B., Lanza, M.R.V., Barros, W.R.P., 2020. Enhanced electrodegradation of the Sunset Yellow dye in acid media by heterogeneous photoelectro-Fenton process using Fe_3O_4 nanoparticles as a catalyst. J. Environ. Chem. Eng. 8, 103621. https://doi.org/10.1016/j.jece.2019.103621.

Pinheiro, V.S., Paz, E.C., Aveiro, L.R., Parreira, L.S., Souza, F.M., Camargo, P.H.C., Santos, M.C., 2019. Mineralization of paracetamol using a gas diffusion electrode modified with ceria high aspect ratio nanostructures. Electrochim. Acta 295, 39–49. https://doi.org/10.1016/j.electacta.2018.10.097.

Poza-Nogueiras, V., Rosales, E., Pazos, M., Sanromán, M.A., 2018. Current advances and trends in electro-Fenton process using heterogeneous catalysts – a review. Chemosphere 201, 399–416. https://doi.org/10.1016/j.chemosphere.2018.03.002.

Ren, G., Lanzalaco, S., Zhou, M., Cabot, P.L., Brillas, E., Sires, I., 2023. Replacing carbon cloth by nickel mesh as substrate for air-diffusion cathodes: H_2O_2 production and carbenicillin degradation by photoelectro-Fenton. Chem. Eng. J. 454, 140515. https://doi.org/10.1016/j.cej.2022.140515.

Salazar, R., Campos, S., Martinez, J., Luna, F., Thiam, A., Aranda, M., Calzadilla, W., Miralles-Cuevas, S., Cabrera-Reina, A., 2022. New development of a solar electrochemical raceway pond reactor for industrial wastewater treatment. Environ. Res. 212, 113553. https://doi.org/10.1016/j.envres.2022.113553.

Salazar, R., Gallardo-Arriaza, J., Vidal, J., Rivera-Vera, C., Toledo-Neira, C., Sandoval, M. A., Cornejo-Ponce, L., Thiam, A., 2019. Treatment of industrial textile wastewater by the solar photoelectro-Fenton process: influence of solar radiation and applied current. Sol. Energy 190, 82–91. https://doi.org/10.1016/j.solener.2019.07.072.

Salmeron, I., Rivas, G., Oller, I., Martinez-Piernas, A., Aguera, A., Malato, S., 2021. Nanofiltration retentate treatment from urban wastewater secondary effluent by solar electrochemical oxidation processes. Sep. Purif. Technol. 254, 117614. https://doi.org/10.1016/j.seppur.2020.117614.

Santos, G.d.O.S., Eguiluz, K.I.B., Salazar-Banda, G.R., Saez, C., Rodrigo, M.A., 2020. Testing the role of electrode materials on the electro-Fenton and photoelectro-Fenton degradation of clopyralid. J. Electroanal. Chem. 871, 114291. https://doi.org/10.1016/j.jelechem.2020.114291.

Segundo, I.D.B., Moreira, F.C., Silva, T.F.C.V., Webler, A.D., Boaventura, R.A.R., Vilar, V. J.P., 2020. Development of a treatment train for the remediation of a hazardous industrial waste landfill leachate: a big challenge. Sci. Total Environ. 741, 140165. https://doi.org/10.1016/j.scitotenv.2020.140165.

Silva, L.G.M., Moreira, F.C., Cechinel, MaA.P., Mazur, L.P., Ulson de Souza, A.A., Souza, S.M.A.G.U., Boaventura, R.A.R., Vilar, V.J.P., 2020. Integration of Fenton's reaction based processes and cation exchange processes in textile wastewater treatment as a strategy for water reuse. J. Environ. Manage. 272, 111082. https://doi.org/10.1016/j.jenvman.2020.111082.

Sirés, I., Brillas, E., 2021. Upgrading and expanding the electro-Fenton and related processes. Curr. Opin. Electrochem. 27, 100686. https://doi.org/10.1016/j.coelec.2020.100686.

Souza, F.L., Rocha, R.S., Ferreira, N.G., Rodrigo, M.A., Lanza, M.R.V., 2019. Effects of coupling hybrid processes on the treatment of wastewater containing a commercial mixture of diuron and hexazinone herbicides. Electrochim. Acta 328, 135013. https://doi.org/10.1016/j.electacta.2019.135013.

Tadayozzi, Y.S., dos Santos, F.A., Vicente, E.F., Forti, J.C., 2021. Application of oxidative process to degrade paraquat present in the commercial herbicide. J. Environ. Sci. Health B 56, 670–674. https://doi.org/10.1080/03601234.2021.1936991.

Thiam, A., Salazar, R., Brillas, E., Sires, I., 2020. In-situ dosage of Fe^{2+} catalyst using natural pyrite for thiamphenicol mineralization by photoelectro-Fenton process. J. Environ. Manage. 270, 110835. https://doi.org/10.1016/j.jenvman.2020.110835.

Thor, S.-H., Ho, L.-N., Ong, S.-A., Abidin, C.Z.A., Heah, C.-Y., Nordin, N., Ong, Y.-P., Yap, K.-L., 2021. Advanced oxidation treatment of amaranth dye synchronized with electricity generation using carbon-based cathodes in a sustainable photocatalytic fuel cell integrated electro-Fenton system. J. Environ. Chem. Eng. 9, 106439. https://doi.org/10.1016/j.jece.2021.106439.

Thor, S.-H., Ho, L.-N., Ong, S.-A., Abidin, C.Z.A., Heah, C.-Y., Yap, K.-L., 2023. Disclosing the mutual influence of photocatalytic fuel cell and photoelectro-Fenton process in the fabrication of a sustainable hybrid system for efficient Amaranth dye removal and simultaneous electricity production. Environ. Sci. Pollut. Res. 30, 34363–34377. https://doi.org/10.1007/s11356-022-24647-5.

Titchou, F.E., Zazou, H., Afanga, H., Jamila, E.G., Akbour, R.A., Hamdani, M., Oturan, M. A., 2022. Comparative study of the removal of direct red 23 by anodic oxidation, electro-Fenton, photo-anodic oxidation and photoelectro-Fenton in chloride and sulfate media. Environ. Res. 204, 112353. https://doi.org/10.1016/j.envres.2021.112353.

Wang, W., Li, Y., Li, Y., Zhou, M., Arotiba, O.A., 2020. Electro-Fenton and photoelectro-Fenton degradation of sulfamethazine using an active gas diffusion electrode without aeration. Chemosphere 250, 126177. https://doi.org/10.1016/j.chemosphere.2020.126177.

Xia, Y., Yang, F., Zhang, B., Xu, C., Yang, W., Li, Y., 2021. Fabrication of novel FeS_2 NWs/Ti_3C_2 cathode for photo-Electro-Fenton degradation of sulfamethazine. Chem. Eng. J. 426, 130719. https://doi.org/10.1016/j.cej.2021.130719.

Xu, A., Brillas, E., Han, W., Wang, L., Sires, I., 2019. On the positive effect of UVC light during the removal of benzothiazoles by photoelectro-Fenton with UVA light. Appl. Catal. B Environ. 259, 118127. https://doi.org/10.1016/j.apcatb.2019.118127.

Xu, J., Olvera-Vargas, H., Loh, B.J.H., Lefebvre, O., 2020. FTO-TiO_2 photoelectrocatalytic degradation of triphenyltin chloride coupled to photoelectro-Fenton: a mechanistic study. Appl. Catal. B Environ. 271, 118923. https://doi.org/10.1016/j.apcatb.2020.118923.

Xu, J., Olvera-Vargas, H., Teo, F.Y.H., Lefebvre, O., 2021. A comparison of visible-light photocatalysts for solar photoelectrocatalysis coupled to solar photoelectro-Fenton: application to the degradation of the pesticide simazine. Chemosphere 276, 130138. https://doi.org/10.1016/j.chemosphere.2021.130138.

Ye, Z., Brillas, E., Centellas, F., Cabot, P.L., Sires, I., 2020a. Expanding the application of photoelectro-Fenton treatment to urban wastewater using the Fe(III)-EDDS complex. Water Res. 169, 115219. https://doi.org/10.1016/j.watres.2019.115219.

Ye, Z., Schukraft, G.E.M., L'Hermitte, A., Xiong, Y., Brillas, E., Petit, C., Sires, I., 2020b. Mechanism and stability of an Fe-based 2D MOF during the photoelectro-Fenton treatment of organic micropollutants under UVA and visible light irradiation. Water Res. 184, 115986. https://doi.org/10.1016/j.watres.2020.115986.

Zhang, S., Chen, C., Li, Y., Geng, J., Li, H., 2024. Effective photo-electrochemical production of H_2O_2 and green Fenton reaction on hierarchical Fe/C/N @ ZIF-8 @ACF for abatement of antibiotics in water. J. Environ. Chem. Eng. 12, 112026. https://doi.org/10.1016/j.jece.2024.112026.

Zhang, Y., Daniel, G., Lanzalaco, S., Isse, A.A., Facchin, A., Wang, A., Brillas, E., Durante, C., Sires, I., 2022. H_2O_2 production at gas-diffusion cathodes made from agarose-derived carbons with different textural properties for acebutolol degradation in chloride media. J. Hazard Mater. 423, 127005. https://doi.org/10.1016/j.jhazmat.2021.127005.

Zhang, Y., Xu, X., Cai, J., Pan, Y., Zhou, M., 2021. Degradation of 2,4-dichlorophenoxyacetic acid by a novel photoelectrocatalysis/photoelectro-Fenton process using Blue-TiO_2 nanotube arrays as the anode. Chemosphere 266, 129063. https://doi.org/10.1016/j.chemosphere.2020.129063.